Recent ultrasound advancements for the manipulation of nanobiomaterials and nanoformulations for drug delivery

Sze Shin Low [a,b], Chang Nong Lim [c], Maxine Yew [d], Wai Siong Chai [e], Liang Ee Low [f,g,h,*], Sivakumar Manickam [i,*], Beng Ti Tey [f,j], Pau Loke Show [b,*]

[a] Continental-NTU Corporate Lab, Nanyang Technological University, 50 Nanyang Drive, Singapore 637553, Singapore
[b] Department of Chemical and Environmental Engineering, Faculty of Science and Engineering, University of Nottingham Malaysia, Jalan Broga, Semenyih 43500, Selangor Darul Ehsan, Malaysia
[c] School of Engineering and Physical Sciences, Heriot-Watt University Malaysia, No. 1, Jalan Venna P5/2, Precinct 5, Putrajaya 62200, Malaysia
[d] Department of Mechanical, Materials and Manufacturing Engineering, University of Nottingham Ningbo China, 199 Taikang East Road, Ningbo 315100, Zhejiang, China
[e] School of Mechanical Engineering and Automation, Harbin Institute of Technology, Shenzhen, Shenzhen 518055, Guangdong, China
[f] Biofunctional Molecule Exploratory (BMEX) Research Group, School of Pharmacy, Monash University Malaysia, Jalan Lagoon Selatan, Bandar Sunway 47500, Selangor Darul Ehsan, Malaysia
[g] Advanced Engineering Platform, Monash University Malaysia, Jalan Lagoon Selatan, Bandar Sunway 47500, Selangor Darul Ehsan, Malaysia
[h] Institute of Pharmaceutics, College of Pharmaceutical Sciences, Zhejiang University, 866 Yuhangtang Road, Hangzhou 310058, Zhejiang, China
[i] Petroleum and Chemical Engineering, Faculty of Engineering, Universiti Teknologi Brunei, Jalan Tungku Link Gadong, Bandar Seri Begawan BE1410, Brunei Darussalam
[j] Chemical Engineering Discipline, School of Engineering, Monash University Malaysia, Jalan Lagoon Selatan, Bandar Sunway 47500, Selangor Darul Ehsan, Malaysia

ARTICLE INFO

ABSTRACT

Recent advances in ultrasound (US) have shown its great potential in biomedical applications as diagnostic and therapeutic tools. The coupling of ultrasound-assisted drug delivery systems with nanobiomaterials possessing tailor-made functions has been shown to remove the limitations of conventional drug delivery systems. The low-frequency ultrasound has significantly enhanced the targeted drug delivery effect and efficacy, reducing limitations posed by conventional treatments such as a limited therapeutic window. The acoustic cavitation effect induced by the ultrasound-mediated microbubbles (MBs) has been reported to replace drugs in certain acute diseases like ischemic stroke. This review briefly discusses the ultrasound principles, with particular attention to the recent advancements in drug delivery applications. Furthermore, ultrasound-assisted drug delivery coupled with nanobiomaterials to treat different diseases (cancer, neurodegenerative disease, diabetes, thrombosis and COVID-19) is discussed. Finally, this review covers the future perspectives and challenges on the applications of ultrasound-mediated nanobiomaterials.

1. Introduction

Human health is one of the major focuses of attention in this century. Despite the continuous progression and scientific advancements in modern medicine, disease detection and therapeutics still need further improvement. In the current situation, drug delivery possesses the issue of not reaching the targeted cells, resulting in poor performance and possibly leading to undesirable adverse effects for the neighbouring healthy cells [1]. Additionally, conventional diagnostic methods are invasive and time-consuming, which could also lead to low accuracy. The term "ultrasound" demonstrates acoustic longitudinal waves with a frequency above the threshold of human hearing (20 kHz). The ultrasound (US) techniques are cost-effective, simple, non-invasive, energy-saving and are emerging tremendously. Conventionally, ultrasound devices are used in object detection and distance measurement and are

---

* Corresponding authors at: Biofunctional Molecule Exploratory (BMEX) Research Group, School of Pharmacy, Monash University Malaysia, Jalan Lagoon Selatan, Bandar Sunway 47500, Selangor Darul Ehsan, Malaysia (L.E. Low); Petroleum and Chemical Engineering, Faculty of Engineering, Universiti Teknologi Brunei, Jalan Tungku Link Gadong, Bandar Seri Begawan BE1410, Brunei Darussalam (S. Manickam); Department of Chemical and Environmental Engineering, Faculty of Science and Engineering, University of Nottingham Malaysia, Jalan Broga, Semenyih 43500, Selangor Darul Ehsan, Malaysia (P.L. Show).

E-mail addresses: low.liangee@monash.edu (L.E. Low), manickam.sivakumar@utb.edu.bn (S. Manickam), PauLoke.Show@nottingham.edu.my, showpauloke@gmail.com (P.L. Show).

typically employed for imaging and diagnostic purposes. Ultrasound can be applied to various fields by tuning the frequency to achieve different

strain COVID-19. In addition, this review suggests the future challenges of ultrasound applications on humans from the engineering perspective

---

Nomenclature

ABCVA	4,4′-azobis(4-cyanovaleric acid)
aFGF	Acidic fibroblast growth factor
Ag	Silver
ARDS	Acute respiratory distress syndrome
Au	Gold
BBB	Blood-brain barrier
BiOCl	bismuth oxychloride
COVID-19	Coronavirus disease
CT	Computed tomography
DESN	Double-effect silica nanoparticle
Dox	Doxorubicin
ELIP	Echogenic liposomes
FUS	Focused ultrasound
fUS	Functional ultrasound
GOx	Glucose oxidase
GV	Gas vesicles
HPS	Hepatopulmonary syndrome
IONP	Iron oxide nanoparticle
LUS	Lung ultrasound
MBs	Microbubbles
MCA	Middle cerebral artery
MPT	Mitochondrial permeability transition
MPTP	1-methyl-4-phenyl-1,2,3,6-tetrahydropyridine
MSC	Mesenchymal stem cell
MSC-EXO	MSC-derived exosomes
MSN	Mesoporous silica nanoparticle
NP	Nanoparticle
PA	Photoacoustic
PEDGMA	Poly (ethylene glycol) dimethacrylate
PFC	Perfluorocarbon
PFC5	Perfluoropentane
PLGA	Poly(lactic-co-glycolic-acid)
PTX	paclitaxel
RGD	Arg-Gly-Asp
RGDS	Arg-Gly-Asp-Ser
ROS	Reactive oxygen species
SARS-CoV-2	Severe acute respiratory syndrome coronavirus 2
SDT	Sonodynamic therapy
STZ	Streptozotocin
TCD	Transcranial Doppler
TEM	Tunnelling electron microscopy
TiO$_2$	Titanium dioxide
tPA	Tissue plasminogen activator
TPP	Triphenylphosphine
UK	Urokinase
US	Ultrasound
UTMD	Ultrasound-targeted microbubble destruction
VEGF	Vascular endothelial growth factor
vWF	von Willebrand factor

---

functions [2-6].

In addition to the diagnostic imaging modality, the energy carried by ultrasound waves could be utilized to influence cell function and drug delivery. The ability to tune ultrasound energy at prefixed intensity has unlocked its potential in therapeutic applications. Ultrasonic-assisted drug delivery has developed progressively and has become popular lately. For drug delivery purposes, ultrasound is relatively non-invasive by controlling the drug release at a desirable location, such as cancer tumours [7-9].

Drug delivery system using ultrasound coupled with nanoparticles (NPs) has resolved the major constraints of conventional drug delivery systems, such as unsatisfactory NPs uptake and accumulation in cells, uncontrolled amount of drug released by NPs and non-targeted delivery [10]. To date, ultrasound has been employed to counter cancer, neurodegenerative disease, diabetes, thrombosis, etc. [11-16]. The combination of NPs and ultrasound has aided in resolving blood clot issues (thrombosis), which is life-threatening if a high dosage of untargeted drugs is employed [17]. The current COVID-19 pandemic is affecting human life globally, with a particular effect on the lung. The non-invasive detection nature of lung ultrasound (LUS) is useful for imaging lung conditions. Recent studies are also focusing on investigating the potential of applying ultrasound-assisted drug delivery for COVID-19 therapy.

Ultrasound in biomedical applications is widely studied, from NPs synthesis to drug delivery. This review presents the recent advancements in ultrasound-assisted drug delivery for various diseases. The fundamentals of ultrasound and their principles related to biomedical applications and the efficacy of ultrasound-assisted drug delivery for different diseases are critically examined. Furthermore, the applications of nanobiomaterial-enhanced ultrasound therapies for different diseases have also been discussed. This review also covers ultrasound development and possible applications to address the latest pandemic virus

and recommends incorporating appropriate functions on nano-biomaterials for enhanced drug delivery efficiency.

2. Mechanism of Ultrasound in Drug Delivery Applications

Ultrasound technology is largely used in sonography (diagnostic imaging) to produce visual images of organs and tissues with high-frequency sound waves for diagnostic purposes, for example, identifying the cause of infection in internal organs and examining the baby in pregnant women. Unlike other imaging modalities (X-ray, CT scan and PET scan), ultrasound does not release ionizing radiation. Hence, it is classified as a non-invasive procedure/treatment and is safely used for pregnant women or infants. The amount of reflected wave is determined by the difference in acoustic impedance between adjacent structures: air, bone, and soft tissue. Strong reflectors such as bones and air appear as hyperechoic images. In contrast, fluid or soft tissue appears as an anechoic or hypoechoic image due to the weak electric current (Fig. 1) [18]. Scattering occurs when the ultrasound waves are redirected at small and rough structures, especially when the acoustic impedance is small. Scattering is responsible for the image texture of the internal organs as it increases at high frequency to provide better resolution (the penetration depth compromises this). Although artefacts generated by refracted ultrasound beam that hits a structure at an oblique angle are generally undesirable as they do not present actual anatomic features [19], however, cases such as lung sonography may provide useful information about the tissue if understood and interpreted correctly by the sonographer [20]. Researchers have utilised the transducer probe used in sonography to induce ultrasound waves to the specific area, triggering ultrasound-assisted material for drug release while observing the treated part for follow-up treatment at the same time.

Besides diagnostic imaging, the advantages of ultrasound have been extended to therapeutic biomedical applications, enhancing the stimuli-
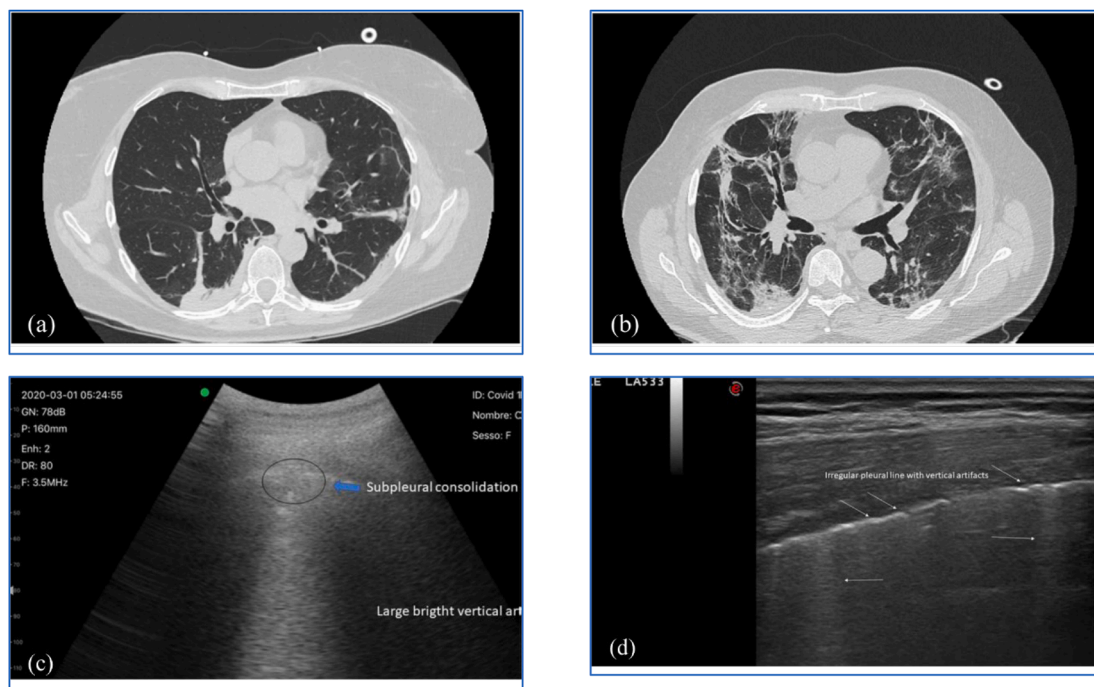
Fig. 1. Ultrasound image of fetal extremities in the second trimester: the hyperechoic femur (thigh's bone), hypoechoic soft tissue and anechoic amniotic fluid. Reprinted from [21] with permission from Taylor & Francis Ltd.

responsive drug delivery (ultrasound-mediated drug delivery). Although researchers continuously investigate the exact mechanism, ultrasound-induced acoustic cavitation has been greatly appreciated in enhancing the therapeutic effect, especially when coupling with micro/nano-bubbles. Acoustic cavitation is the formation, growth and collapse/implosion of microbubbles (MBs) induced by ultrasound waves. When ultrasound passes through a liquid medium, the dissolved gas nuclei normally contained in the liquid medium start to grow and collapse due to mechanical vibration [22]. The oscillation and implosion of these cavitation bubbles introduce several physical effects such as the sudden rise of temperature, shock waves, shear force, mechanical stress and free radical production. This phenomenon is the main mechanism in enhancing targeted drug delivery by ultrasound.

Acoustic cavitation is induced by ultrasound waves, activating the gas nuclei in the medium/tissues and vessels. This effect can be greatly enhanced by the addition of MBs such as perfluorocarbon (PFC) gas and echogenic liposomes (ELIP) [23]; the cavitation activity of these MBs depends on their size, shell, and resonance frequency. The combined low-frequency ultrasound wave with MBs to trigger cavitation is known as ultrasound-targeted microbubble destruction (UTMD) and has been utilised by researchers in therapeutic applications [24]. UTMD induced cavitation can enhance the permeability of natural barriers such as skin and cell membranes, thus increasing the uptake of drugs. In addition, the ultrasound wave applied can trigger the release of the encapsulated drugs for localised treatment. The mechanism of ultrasound-mediated drug delivery mainly relies on acoustic cavitation. It has been used to treat various diseases via different routes such as sonoporation, sono-dynamic therapy (SDT), sonophoresis, and sonothrombolysis.

Sonoporation refers to the formation of pores in the cell membrane upon exposure to ultrasound waves, enhancing the membrane permeability for intracellular transfer [25]. Studies have shown that sonoporation mechanisms were mainly due to transient cavitation caused by high-intensity ultrasound (>1 MPa, 1 MHz), leading to microstreaming and shear stresses related to stable oscillations [26,27]. The asymmetric implosion of MBs increases the permeability of the surrounding vessel walls and cell membranes, facilitating gene and drug delivery. In vitro experiments have shown that the dissolved gas in the culture medium is sufficient to generate cavitation bubbles; however, *in vivo* application required the addition of micro and nanobubbles to induce sonoporation as human lungs are efficient in clearing small bubbles from the circulatory system [28]. In vitro and *in vivo* oncological research has shown increased uptake of anti-cancer drugs such as bleomycin, adriamycin, and cisplatin through sonoporation [21,29,30]. Also, low-frequency ultrasound has been reported to temporarily disrupt the blood–brain barrier (BBB) and enhance drug diffusion through MBs. The targeted BBB disruption supports the delivery of chemotherapeutic agents to brain tumours that usually cannot penetrate through. Focused ultrasound ranging from 0.5 to 4 MHz have shown efficient gene transfer with one or two orders magnitude higher than using plasmid DNA alone [31,32].

SDT has emerged as a novel approach for non-invasive targeted cancer treatment, involving the sensitization of target tissues with sonosensitizer. This non-toxic sensitizing chemical agent can be activated upon exposure to low-intensity ultrasound [33]. Yumita and Umemura first reported hematoporphyrin, a well-known photosensitizer activated by ultrasound-induced cavitation to generate anti-tumour effects [34,35]. Sonosensitizer can be activated by low-intensity ultrasound to produce reactive oxygen species (ROS) via three methods: (1) light through the sonoluminescence process [36] (2) pyrolytic reactions (3) increase in the acoustic cavitation effects [37], presenting advantages such as higher tissue penetration depth over photodynamic therapy [38]. The presence of MBs has also been reported to significantly enhance the thermal effects, perturbing the tumour vasculature, with the role as the carrier of molecules and as contrast agents for diagnostic imaging [39]. Though studies have demonstrated the therapeutic efficacy of SDT based on ROS generation and mechanical cytotoxic effects, the mechanism behind the cytotoxic effects is still lacking. Canavese et al. reviewed and discussed the possible processes governing the observed cytotoxic effects [40]. Considering cavitation bubbles which act as nanometric sonochemical reactors during implosion (generating extremely high temperature and pressure), ROS was generated by direct pyrolysis or pyrolysis of water molecules where chemical reaction can occur inside or near the surrounding of the imploding bubbles [41]. The minimum ultrasound intensity required to generate transient cavitation,

known as cavitation threshold, depends on the characteristics of the irradiated medium. The presence of NPs has been demonstrated to decrease the cavitation threshold and initiate inertial cavitation near the target cell to elicit cytotoxic effects at low intensity [42]. Transient cavitation has been concluded as the key mechanism behind the therapeutic effects of SDT [36].

Sonophoresis refers to ultrasound-mediated transdermal drug delivery. The ultrasound waves have greater penetration depth than iontophoresis, able to penetrate up to 4 to 6 cm into the tissues. Several mechanisms, including cavitation, thermal effects, induction of convective transport and mechanical effects such as stress due to pressure variation, have been hypothesized. However, experimental findings showed that the cavitation effect is the dominant mechanism in enhancing drug delivery. The cavitation effect can occur inside and outside the skin but studies have reported that cavitation outside the skin has an insignificant effect on sonophoresis [43,44]. Cavitation can occur in various biological tissues due to the pre-existing gas nuclei trapped in the intracellular and intercellular structures, mostly present in the keratinocytes. The oscillation of cavitation bubbles near the keratinocyte-lipid bilayer interfaces and the shock waves from the collapse of cavitation bubbles leads to structural disordering, enhancing the permeation of drugs through the stratum corneum [45-47]. Studies have also reported on increasingly difficult to generate cavitation at high frequency due to the short duration of the oscillating acoustic pressures, diminishing diffusion into cavitation nuclei [48,49].

Sonothrombolysis has been found to enhance the lysis rate of the blood clots under low-frequency ultrasound. The cavitation effect temporarily loosens the fibrin clot and increases the diffusion of thrombolytic drugs into the blood clot. The thrombolytic treatment can be further improved by combining with the aid of thrombus targeted MBs which increases the surface area of the thrombus by the mechanical shear stress induced by the ultrasound. The role of acoustic streaming in encouraging diffusion, transporting thrombolytic agents, and mechanical perturbation have been proposed [50-54]. Ultrasound irradiation also mediates fibrin disaggregation and induce biological effects such as limiting the enzyme activation and platelet activation [55-59]. Apart from the cavitation effect, most studies have reported an insignificant relationship between the thermal mechanisms and thrombolytic outcomes [60-62]. The experimental findings demonstrated an increase in the thrombolytic effect only with ultrasound and MBs without thrombolytic drugs, further concluding the importance of the UTMD cavitation effect [63,64].

3. Ultrasound-assisted delivery of nanobiomaterials for biomedical applications

US is one of the externally applicable stimuli employed for a wide range of applications. It involves the continuous generation and violent implosion of cavitation bubbles to produce intense local pressure, heating and oxidative radicals, giving rise to thermal or mechanical stimulation of nanomaterials to aid their delivery efficacy to the diseased sites [65]. As a result, US could induce: (1) the instability of nanomaterials, (2) controlled drug release (3) enhancement of the permeability of nanomaterials across biological barriers. Besides, US could also be used under less violent mode where stable cavitation bubbles oscillate around an equilibrium size could be generated to avoid unwanted damage to the surrounding [66,67], allowing their employment for medical diagnosis based on the difference in the absorbance of ultrasound by the tissues [66]. The following sections disclose ultrasound's performance in mediating nanomaterials' delivery for various biomedical applications, including cancers, neurodegenerative diseases, diabetes, thrombosis and coronavirus disease 2019 (COVID-19) (Table 1).

3.1. Cancer

Cancer is a lethal disease that arises from abnormal genetic mutation or uncontrollable cell proliferation [112], which remains one of the major causes of mortality worldwide, with a continuous increase in new cases [113]. US has been an emerging tool for the diagnosis and treatment of cancers. It could be applied to control the release of drugs at the tumour site, thus preventing potential toxicity or irritation of healthy tissues, which are commonly observed in conventional chemotherapeutic and radiotherapeutic treatments of cancer. US-triggered tumour-specific drug release could be achieved by incorporating thermosensitive ligands into the nanomaterial [68,114]. Paris et al. prepared mesoporous silica nanoparticles (MSNs) decorated with PEG and thermal sensitive 4,4′-azobis(4-cyanovaleric acid) (ABCVA) [68]. Upon US-induced heating, the ABCVA linker was cleaved, resulting in the exposure of the positively charged MSN to enable effective cell internalization and tumour-targeted release of topotecan. The successful delivery of the anticancer drug topotecan has significantly reduced human osteosarcoma (HOS) cells' viability compared to control samples. However, *in vivo* animal study is necessary to verify the practicality of the asprepared nanosystem further. It should also be noticed that the MSN indicated in the examples required a timely (>1 day) fabrication of core nanomaterials, followed by subsequent surface functionalization. Indeed, the sonochemical method has previously been reported to be feasible for the synthesis of similar quality MSN in few hours with controllable physicochemical properties under different ultrasonic conditions [115]. Hence, the employment of US would be useful for more efficient and time-saving fabrication of nanomaterials for biomedical applications. In another study, Song and colleagues ultrasonically synthesized PFC nanoemulsions to perform US-triggered modulation of the hypoxic microenvironment around tumours [69], as inspired by the ability of PFC to release encapsulated oxygen upon photothermal stimulation [116]. The PFC nanoemulsions are first intravenously injected into 4 T1 tumour-bearing mice and allowed to load oxygen through lung capillary based on their long blood circulation time and high oxygen solubility. Upon arrival at tumour sites, the application of US waves further triggers the burst release of oxygen from the nanoemulsions, contributing to the combating of hypoxia-related resistance in cancer therapy. Several reports also revealed the use of ultrasonic mechanical effects to achieve tumour-targeted nanomaterial deformation and drug release. As shown in Fig. 3a, a double-effect silica NP, comprising hydrophobically modified MSN, folic acid-conjugated β-cyclodextrin (β-CD) and paclitaxel (PTX), has been constructed and utilized for US-assisted drug delivery [70]. FA-β-CD functions not only for the targeting of folate receptor (rich on tumour surface) but also to block the pores of MSN to avoid the premature leakage of PTX. After the intracellular internalization of double-effect silica nanoparticle (DESN) into tumour cells, US was used to degenerate FA-β-CD, releasing PTX for tumour chemotherapy. In addition, increasing the US intensity led to a higher release of PTX and toxicity to tumour cells (Fig. 3b and c), suggesting the importance of US to manipulate the nanocarrier for enhanced tumour therapy. In vivo analysis with nude mice further revealed the excellent performance of the DESN for inhibiting tumour growth. Besides, US-controllable liposomes have also been developed to deliver chemotherapeutic drugs such as doxorubicin (Dox) [71]. The US-assisted liposome contained a perfluoropentane (PFC5) nanoemulsion and Dox (eLipoDox). The PFC$_5$ nanoemulsion was observed to turn into gas bubbles and cavitate upon US irradiation, inducing Dox release from the liposome.

Dox has been reported to promote side effects such as platelet aggregation and adhesion to endothelial cells [117], oxidative stress, cardiomyocyte apoptosis, mitochondrial dysfunction, leading to thrombosis disease and heart failure [72]. In a typical assay, oxidative stress contributes to the formation of excess free radicals. Hence, the lipid oxidation can be evaluated by measuring the level of superoxide dismutase (SOD, an antioxidant enzyme that decreases with oxidative

Table 1

Summary of nanomaterials associated with US-assisted delivery for various biomedical applications.

| Biomedical application	Nanomaterial	Functional component	Function	Tested model	Remark	Ref.
Cancer	Topotecan-loaded ABCVA-PEG-MSN	ABVCA	Thermosensitive drug release	HOS cell	US-heating triggered the release of topotecan for tumour elimination.	[68]
	Albumin-stabilized PFC nanoemulsion	PFC	US-triggered oxygen release to combat hypoxia	4 T1 tumour-bearing mice	US-triggered release of oxygen from PFC nanoemulsion to modulate hypoxic tumour environment for improving PDT.	[69]
	DESN	MSN	Cavitation-induced drug release	4 T1 tumour-bearing mice	Gas stored in the pores of MSN enhanced the cavitation effect to release the loaded PTX for tumour chemotherapy.	[70]
	eLipoDox	PFC5 nanoemulsion	Cavitation-induced drug release	HeLa cell line	PFC5 nanoemulsion turns into gas bubbles and cavitates to release Dox from the liposome.	[71]
	aFGF-NPs and cationic lipid MBs	Cationic lipid MBs	UTMD-assisted drug delivery	Dox-injected heart failure mice	The UTMD of MB resulted in the enhanced delivery of aFGF-NP to attenuate the Dox-induced heart failure	[72]
	FeN@GOx@M and MBs	MBs	UTMD-assisted drug delivery	A2780 tumour-bearing mice	The UTMD of MB resulted in the enhanced penetration of FeN@GOx@M into tumours.	[73]
	PION@Ce6	IONP, Ce6	SDT	H22 hepatocellular carcinoma cell line	IONP reduces the cavitation threshold to improve the sonosensitivity of Ce6.	[74]
	TiO_2	TiO_2	SDT	C32 melanoma-bearing mice	TiO_2 produces ROS for tumour SDT in the presence of ultrasound.	[75]
	Au-TiO_2-A-TPP	TiO_2	SDT	MCF-7 tumour-bearing mice	Au coating increased the ROS generation by TiO_2.	[76]
	C-TiO_2 NPs	TiO_2	SDT	4 T1 tumour-bearing mice	Carbon doping increased the ROS generation by TiO_2.	[77]
	V-TiO_2 nanospindle	TiO_2	CDT-SDT	4 T1 tumour-bearing mice	Vanadium doping not only increased ROS produced by TiO_2 but also catalysed the degradation of H_2O_2 into ROS.	[78]
	DLMB	MB, DVDMS	SDT	4 T1 tumour-bearing mice	MB undergo cavitation, leading to a higher release of DVDMS to produce more ROS.	[79]
	RB-MB	MBs	US imaging-guided SDT	HT-29 tumour-bearing mice	MB prevented the premature release of ARB and increased its retention in tumours for enhanced SDT.	[80]
	GV	Anabaena flos-aquae derived GV	US imaging	SCC7 tumour-bearing mice	PEG improved the colloidal stability of GV, while HA enhanced the accumulation of GV in the tumour.	[81]
	MB$_{iRGD/CCR2}$	MBs	US imaging, gene delivery	MCF-7 tumour-bearing mice	Dual targeting ability improved the tumour specificity of MB for US imaging and gene delivery.	[82]
	FA-CS-GO	GO	PA imaging	MDA-MB-231 tumour-bearing mice	FA assisted in tumour targeting for improved PA imaging and PTT of the tumour.	[83]
	Porphyrin-based MB	Porphyrin NPs s	US and PA imaging	KB xenograft-bearing mice	US-implosion of MB into porphyrin NPs for US (using encapsulated gas bubble) and PA (using porphyrin) dual imaging.	[84]
Neurodegenerative disease	Qc@SNPs-MB	MBs	FUS BBB opening	AD mice	Cavitation of MB increased permeability of Qc@SNP across BBB for quercetin delivery.	[85]
	LpDNA-MB	MBs	FUS BBB opening	MPTP-treated PD mice	Cavitation of MB increased permeability of LpDNA across BBB for gene delivery.	[86]
		PFC5 nanoemulsion	US-triggered propofol release	Pentylenetetrazol-treated mice		[87]

Table 1 (*continued*)

Biomedical application	Nanomaterial	Functional component	Function	Tested model	Remark	Ref.
	Propofol-loaded micelle-stabilized PFC5 nanoemulsion				US cavitation released the encapsulated propofol to silence epileptic seizures.	
	PX@OP@RVG	PX	SDT and chemotherapy	APP/PS1 transgenic mice	Successful delivery of PX for SDT and chemotherapy of AD.	[88]
	BiOCl nanosheet	BiOCl	SDT	5xFAD mice	US-triggered piezoelectric polarization to produce ROS.	[89]
	Iodide-doped Ag-AuNR	Ag	PA imaging	Zymosan-treated murine model	Ag oxidized by RONS, leading to the reactivation of the PA signal of Au.	[90]
	TPP-HCy-BOH	HCy	PA imaging	Lipopolysaccharide-treated mice	H_2O_2-induced reactivation of PA signal of HCy.	[91]
	MBs	MBs	fUS imaging		MB compensate the US signal attenuated by the skull to improve the mapping of brain vasculature.	[92]
	GV	Anabaena flos-aquae derived GV	fUS imaging	C57BL/6J	Amplified US signal with reduced signal fluctuation than MB contrast agent.	[93]
	MBs	MBs	fUS imaging	Human trial	Deep vasculature imaging to characterize blood-flow dynamics with resolution up to 25 μm.	[94]
Thrombosis	PEG-gelatin loaded with tPA	PEG-gelatin	US triggered drug release; cavitation induced thrombolytic effect	Rabbit thrombosis model-right femoral artery	Thrombolytic drug activity is initially suppressed by PEG-gelatine and released upon exposure to ultrasound.	[95]
	tPA-gelatin and zinc ions complex NPs	Basic gelatin and zinc structure	US triggered drug release; cavitation induced thrombolytic effect	Swine acute myocardial infarction model	Thrombolytic drug activity is initially suppressed by gelatine NPs and released upon exposure to ultrasound.	[96]
	tPA-loaded ELIP	ELIP	US triggered drug release	Rabbit acute aorta clot model	Ultrasound enhances drug release to increase the thrombolytic effect.	[97]
	PFC gas containing ELIP coated with RGD peptides (tPA)	ELIP	US triggered drug release; cavitation induced thrombolytic effect	Iliofemoral arteries thrombosis rabbit	Ultrasound cavitation enhances the thrombolytic effect, and thrombus targeted RGD peptides increase the drug release effect.	[98]
	Magnetically targeted MBs (tPA)	Magnetic MBs	US induced thrombolytic effect enhanced by the magnetic MBs	In vitro porcine blood clots in partially occluded middle cerebral artery	Ultrasound induced thrombolytic effect; magnetic MBs attached to the surface of thrombus to enhance the thrombolytic action.	[99]
	Sulfur hexafluoride MBs (tPA)	MBs	US enhanced cavitation effect	Rabbit model of middle cerebral artery occlusion	US cavitation on the MBs accelerated the thrombolysis effect.	[100]
	Galactose MBs (tPA)	MBs	US enhanced cavitation effect	Patients with acute stroke attributable to MCA occlusion	US cavitation on the MBs accelerated the thrombolysis effect.	[101]
	Perflutren-lipid microspheres (UK)	MBs	US enhanced cavitation effect	Stroke subjects treated within 3 h had abnormal thrombolysis in brain ischemia	US cavitation on the MBs accelerated the thrombolysis effect.	[102]
	RGDS coated MBs, SonoVue (UK)	MBs	US enhanced cavitation effect	Rabbit with femoral arterial thrombosis	US cavitation on the MBs accelerated the thrombolysis effect.	[103,104]
Diabetes	Drug loaded polyanhydrides, polyglycolides, and polylactides	Biodegradable polymer matrices and nonerodable ethylene/vinyl acetate copolymer	Cavitation-induced drug release	Rats	Ultrasound enhanced polymer degradation to release the incorporated drugs.	[105]
	Insulin-loaded pHEMA/PEGDMA 0.4 K copolymer	C12 methylene chains	Cavitation-induced insulin release	In vitro 3 T3-L1 adipocyte cells	US irradiation distorts the C12 chain to release insulin.	[106]
	Nano-network consist of alginate coated PLGA and chitosan-coated PLGA	Particle-particle interaction	Cavitation-induced insulin release	STZ-induced type 1 mice	Shock waves from inertial cavitation facilitate rupture of polymer chains in PLGA, releasing insulin upon US exposure.	[107]
	Insulin-loaded PLGA coated by chitosan microgel	Chitosan microgel	Cavitation-induced insulin release	STZ-induced type 1 mice	Improved performance on pulsatile release profile due	[108]

Table 1 (*continued*)

Biomedical application	Nanomaterial	Functional component	Function	Tested model	Remark	Ref.
					to "recharge" capability of chitosan microgel.	
	VEGF gene containing lipid-stabilised MBs	MBs	UTMD-assisted gene delivery	STZ-induced type 1 mice	Improve the efficacy of islet transplantation to restore the function of pancreatic beta-cell in releasing insulin.	[109]
COVID-19	MBs from agitated saline	MBs	US imaging to detect intracardiac/ intrapulmonary shunting	Covid-19 patients	TCD was used to detect and quantify MBs appearing in the cerebral circulation to define the disease severity.	[110]
	MSC-EXO loaded polymer-based encapsulated MBs	Polymeric matrices	US-triggered drug release from polymeric vesicles	Simulation on human lung model	Polymeric MBs rupture upon US exposure to release the MSC-EXO for lung damage treatment.	[111]
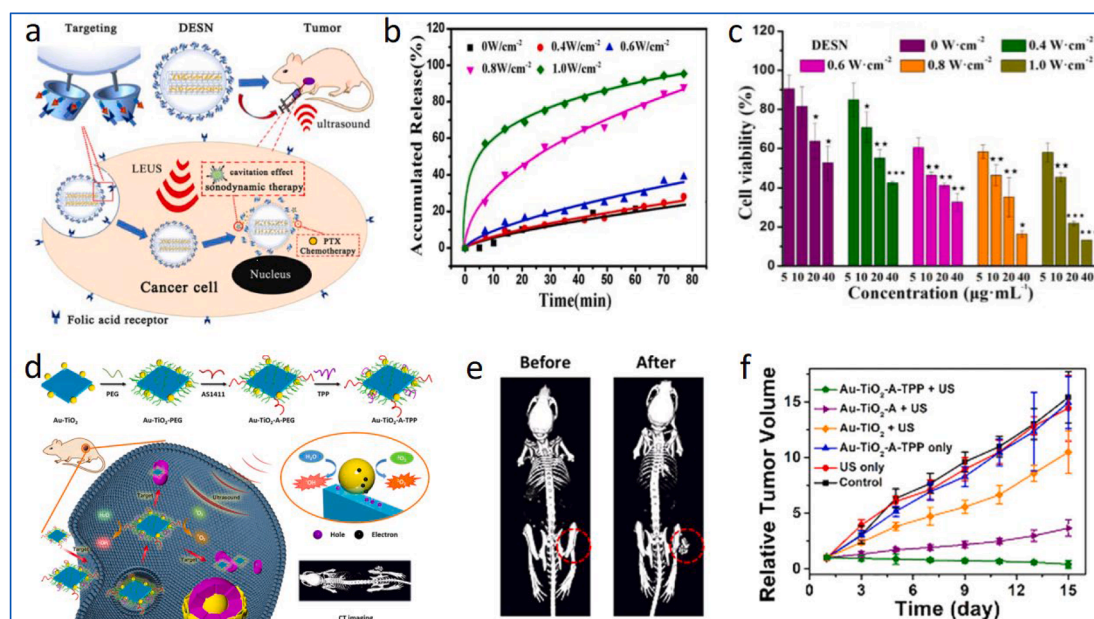
Fig. 3. (a) Schematic representation of the tumour-targeting process of DESN for subsequent US-triggered release of PTX for chemo-SDT of tumours (b) The release profile of PTX from DESN under US sonication at different intensities (c) Cell viability of 4 T1 cells upon incubation with different concentrations of DESN without/ with US irradiation at different power (d) Schematic diagram of the synthesis and CT imaging-guided SDT of Au-TiO$_2$-A-TPP (e) CT images of mice before and after the intravenous injection of Au-TiO$_2$-A-TPP (f) Changes in tumour volume of the MCF-7 tumour-bearing mice subjected to different treatment groups. Reprinted from [70,76] with permission from the authors (CC BY license) and the American Chemical Society.

stress) and malondialdehyde (MDA, a marker of lipid peroxidation) [72]. Besides, overwhelmed ROS also opened the mitochondrial permeability transition (MPT) pore, which initiated the release of apoptosis factors and, eventually, mitochondrial dysfunction and apoptosis [118]. Recently, Zhou et al. proposed the combinational use of UTMD and acidic fibroblast growth factor (aFGF) to attenuate the heart failure caused by Dox (a drug for tumour chemotherapy) [72]. The authors first prepared the aFGF-NPs and cationic lipid MBs and further employed them for UTMD-mediated anti-heart failure cardioprotection. The aFGF is known to facilitate angiogenesis, attenuate myocardial ischemia and improve cardiac function due to its ability to proliferate vascular endothelial cells and smooth muscle cells [119]. With the aid of UTMD, the combinational delivery of aFGF-NPs and cationic lipid MBs endowed the reduced lipid peroxidation (amplified SOD and lowered MDA) in myocardial tissue and the elevated Bcl-2 protein level (a known apoptosis regulator where its increment could inhibit apoptosis). On the other hand, the myocardium of Dox-induced heart failure is accompanied by a low capillary density. It could be recognized through the decrease in platelet-endothelial cell adhesion molecule (CD31)

expression. The UTMD-assisted delivery of aFGF- NPs in Zhou's work successfully increased the CD31 expression and the blood vessel density in ischemic myocardium, suggesting the as-developed formulations (aFGF-NPs + cationic lipid MBs + UTMD) to be promising for the treatment of Dox-facilitated heart failure [72].

The UTMD-enhanced delivery is believed to be due to MB's destruction, which enhances the permeability of nanomaterials across tumour vessel walls and cell membranes. Recently, Xiang et al. demonstrated the enhanced delivery of Fe-metal organic framework (MOF)-based nanozyme (FeN) to tumour sites with the help of UTMD [73]. The FeN is first coated with glucose oxidase (GOx) and tumour cell membrane to yield a tumour-targeting nanozyme (termed FeN@-GOx@M). Here, the GOx is expected to catalyse the conversion of glucose to gluconic acid and H$_2$O$_2$, which supplemented the nanozyme-induced Fenton-like reactions to produce ROS for tumour elimination. To improve the penetration of the nanozyme into the tumour, MBs have been co-injected along with the FeN@GOx@Ms intratumorally into A2780 tumour-bearing nude mice to induce UTMD, where the latter enhanced the penetration of the FeN@GOx@M into the tumour, thus

improved the inhibition of tumour growth as compared to the control.

SDT is another known technique involving the combined usage of low-intensity US and sonosensitizers to generate ROS for tumour elimination [40,120]. SDT utilizes the advantage of US waves that exhibit high specificity and deep tumour penetrability to activate the sonosensitizers after their accumulation in the tumour, realizing tumour-specific elimination with minimal influences to healthy tissues [40,120]. Despite their potential for tumour treatment, conventional sonosensitizers suffer from several limitations. For instance, they indiscriminately attack the tissues regardless of the malignancy status since they are mostly derived from photosensitizers (Chlorin e6 (Ce6), photofrin, etc. [121]), or chemotherapeutic drugs (Dox, levofloxacin, etc. [122,123]), which could impart severe irritation or toxicity to healthy tissues [124]. On the other hand, conventional sonosensitizers are inherently hydrophobic and could aggregate easily based on a hydrophobic interaction, leading to poor aqueous solubility and decreased ROS productivity [124]. Fortunately, such obstacles could be addressed by integrating NPs as a carrier to deliver the sonosensitizers. As evidenced in the study of Zhang et al., PEGylated iron oxide NP (IONP) has been used to chemically bond Ce6 (yielding PION@Ce6) to improve its sonosensitivity [74]. The presence of PEG improved aqueous solubility and colloidal stability. Meanwhile, IONP reduced the cavitation threshold for enhanced ROS production by providing a nucleation site for cavitation [125]. As a result, in the presence of US, PION@Ce6 showed supreme reduction in cell viability of H22 hepatocellular carcinoma cell lines as compared to free Ce6, reflecting an improved sonosensitivity.

Apart from serving as a carrier, some NPs can work as the sensitizer itself with US assistance. Titanium dioxide (TiO_2) NP is one of the foremost sonosensitizers for SDT due to its high biocompatibility, stability and low toxicity. The first evidence concerning the performance of TiO_2 against tumours was reported by Harada and colleagues [75]. In the performed study, no cell viability reduction was observed upon subjecting the C32 tumour melanoma cells to incubation with TiO_2 in the absence of ultrasound. In contrast, the introduction of ultrasound triggers TiO_2 to produce ROS, reducing the cell viability of C32 tumour melanoma cells. Similar observations have been disclosed under the *in vivo* mice model test. The tumour reveals an approximately 2.5-fold smaller volume than the untreated mice, suggesting the efficacy of TiO_2-mediated SDT for tumour elimination.

Nevertheless, native TiO_2 is associated with low ROS generation efficiency due to its wide bandgap and rapid recombination of electrons and holes in the band structure [126]. The latter has been addressed via the surface modification of TiO_2 with noble metal to promote the transfer of an interfacial electron to prevent electron-hole recombination [76]. Cao et al. coated Au nanocrystal, PEG, triphenylphosphine (TPP) and AS1411 aptamer onto TiO_2 nanosheets (Au-TiO_2-A-TPP) for mitochondria-targeted SDT (Fig. 3d) [76]. While the PEG layer increases the colloidal stability of the nanosheet, Au-TiO_2-A-TPP first utilizes AS1411 aptamer to pass through the cancer cell membrane. TPP was then responsible for further internalization in mitochondria for subsequent US-induced ROS generation, causing cell apoptosis. Both *in vitro* and *in vivo* tests showed promising tumour suppressing outputs using the designed formulation (Fig. 3e). Notably, the presence of Au also makes CT imaging possible (Fig. 3f), suggesting the imaging-guided SDT using the as-developed Au-TiO_2-A-TPP. Besides noble metal compounding, Yang et al. improved the SDT performance of TiO_2 NPs based on carbon doping, where the latter lowered the bandgap of TiO_2 to ease the release of energy to generate ROS [77]. Intriguingly, the carbon-doped TiO_2 (C-TiO_2) NPs successfully inhibited the proliferation of 4 T1 breast tumours *in vivo*, resulting in an approximately 3-fold reduction in tumour volume than control samples. Wang et al. reported the conjugation of TiO_2 with vanadium to yield V-TiO_2 nanospindle for combined chemodynamic therapy (CDT)-SDT of tumours [78]. Besides SDT-mediated by TiO_2, the nanostructured vanadium act as a nanozyme to catalyse the degradation of H_2O_2 into ROS. Vanadium doping also facilitates the narrowing of the

bandgap of TiO_2 to improve ROS production. The synergistic effects of the combined therapies favoured ROS overexpression, depleting the GSH content around the tumour and eventually inhibiting tumour growth in mice models.

Noteworthily, recent studies have demonstrated that incorporating MBs alongside sonosensitizers could lead to higher ROS generation than the sonosensitizer alone as the MBs could provide nuclei for cavitation initiation, eventually leading to sonoluminescence emission that excites the nearby sonosensitizer [127]. Moreover, the high local temperature generated from cavitation also causes pyrolysis reactions, increasing ROS production [80]. Li et al. loaded sinopporphyrin sodium (DVDMS) into liposomes and further conjugated DVDMS liposomes with MBs through biotin-avidin linkage to yield DVDMS liposome-MB complexes (DLMBs) for enhanced SDT against breast cancer [79]. Under US exposure, cavitation of MB is observed, increasing the release of DVDMS to generate more ROS than the control groups (with mere DVDMS liposome), resulting in higher SDT performance under both cellular and animal studies. Nevertheless, the *in vivo* delivery of DLMB in the study depends solely on US-enhanced diffusion and enhanced permeation and retention. Since MB is often used as an echo-enhancer for US imaging, the inclusion of MB may also give rise to possible imaging of the SDT process. Hou et al. demonstrated US imaging-guided SDT for tumour treatment [80]. The authors conjugated rose bengal with dihexadecylamine via amine linkage to yield amphiphilic rose bengal (ARB). Then, ARB, together with sorbitan monostearate (Span-60) and polyoxyethylene (40) stearate (PEG-40S), were used to produce MBs containing fluorinated gas (RB-MBs). The size of the MBs could be reduced to the nanoscale with the assistance of US, facilitating their higher accumulation in tumour sites, attributed to both the reduced size and the sonoporation effect. The improved intracellular penetration thus allowed the successful *in vivo* US imaging using a 5 MHz clinical US scanner. As for therapy, a lower frequency US (1 MHz) was employed to ensure cavitation initiation. The *in vivo* application of RB-MBs in tumour-bearing mice showed maximum tumour growth inhibition up to 76.5% compared to those treated with rose Bengal + US (49.2%). Overall, the *in vivo* outputs indicated the enhanced SDT effect against cancer due to MBs and disclosed the successful US imaging-guided SDT of tumour. It is suggested that the investigation to include tumour-targeting moieties in the formulation could be performed in the future to strengthen the practicality of MB systems for tumour therapy.

Besides therapeutic approaches, US has also been utilized to imaging tumours based on the difference in the absorbance of US by soft tissue [66], where the differences could be enhanced using US contrast agents, such as micro/nano-bubble liquid emulsion and solid NPs. Wang and colleagues reported the use of nanobubbles for US imaging of tumours [81]. In the study, gas vesicle harvested from the cyanobacteria has been utilized as the core of the nanobubble. Nevertheless, native gas vesicles (GVs) are prone to rapid clearance (84 % cleared in 20 min) by the reticuloendothelial system (RES) that limits their potential for tumour imaging. To produce tumour-targetable nanobubbles with enhanced *in vivo* stability, the authors covalently conjugated hyaluronic acid (HA) and PEG onto the GVs to enable tumour CD44 receptor-targeting and improve colloidal stability, respectively (Fig. 4a). The formulation lengthened the retention time of the GVs to over 48 h. It revealed tumour-specific accumulation of the GVs *in vivo*, which realizes their potential for tumour-specific US imaging (Fig. 4b). US imaging could also be used for imaging-guided tumour therapy due to its real-time imaging capabilities. Liu et al. demonstrated US-imaging guided tumour gene therapy using DNA-loaded MBs [82]. The MBs was integrated with PEI to gain cationic characteristics, allowing the loading of negatively charged pGPU6/GFP/shAKT2 plasmid DNA.

Further, the tumour-targeting ability was granted via the biotin-avidin linkage-mediated immobilization of iRGD peptides (cyclo(Cys-Arg-Gly-Asp-Lys-Gly-Pro-Asp-Cys) and CCE2 (chemokine (C–C motif) receptor 2) antibodies. The embodiment of the two tumour-targeting ligands favoured the higher accumulation of the as-prepared MB
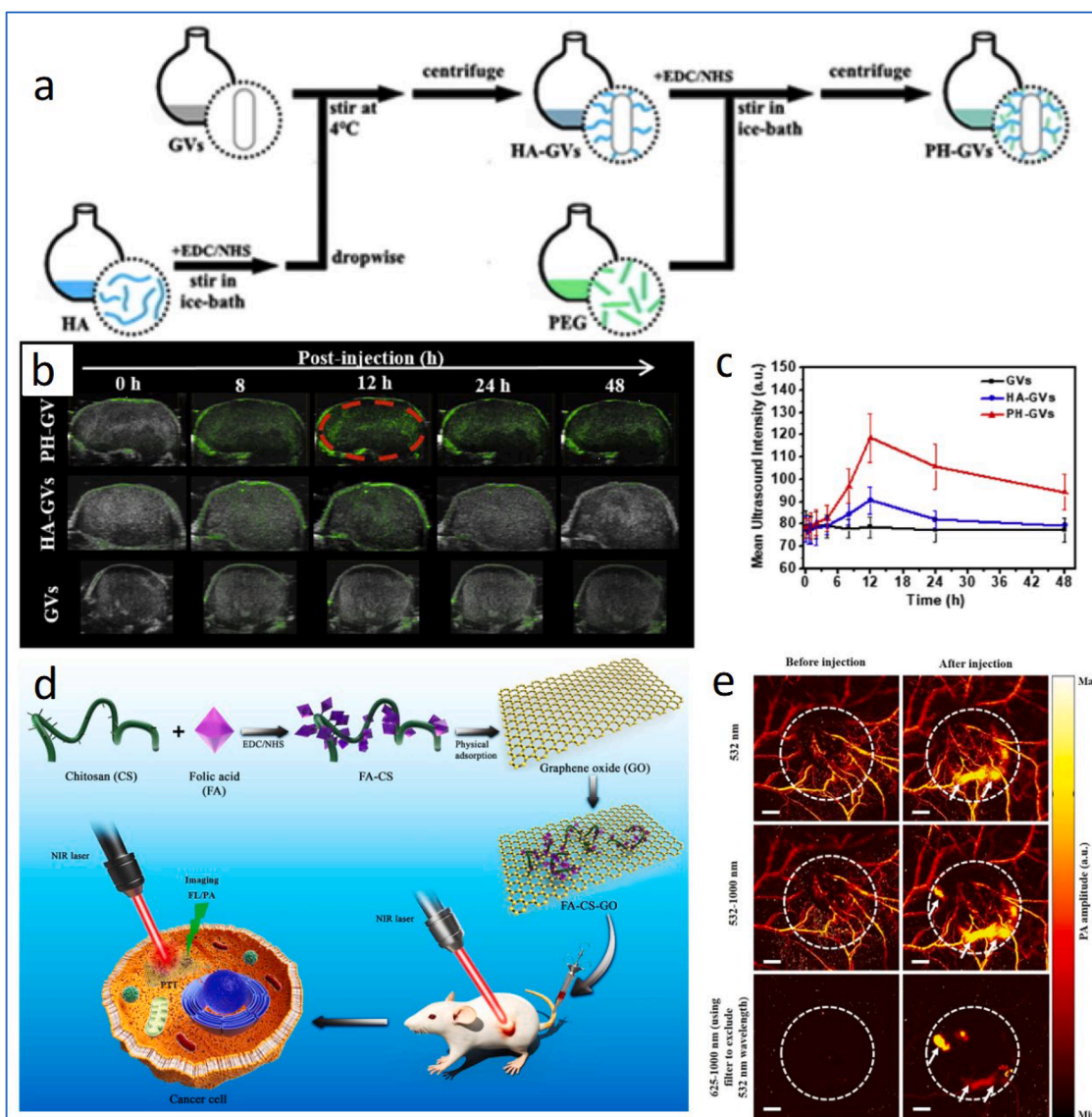
Fig. 4. (a) Schematic illustration of the preparation of PEGylated HA-GVs (PH-GVs). (b) US images of GVs, HA-GVs and PH-GVs in tumour sites upon intravenous injection with different formulations and (c) their respective quantitative intensity. (d) Schematic showing the preparation and PTT of FA-CS-GO. (e) In vivo PA images of tumour tissue before and after the introduction of FA-CS-GO under 532, 532–1000 and 625–1000 nm scanning. White dash lines indicating the tumour area. Scale bar = 2 mm. Reprinted from [81,83] with permission from Elsevier.

(denoted MB$_{iRGD/CCR2}$) around tumour sites, promoting US contrast signals *in vivo*. Notably, with the concurrent utilization of sonoporation, the encapsulated DNA has been successfully delivered and released in tumours to silent the AKT2 protein expression to inhibit tumour growth.

Recently, a hybrid-imaging modality, photoacoustic (PA) imaging, detects the acoustic waves generated from the thermoelastic expansion and contraction of haemoglobin due to nanosecond pulsed light exposure for tumour imaging [128,129]. The combination of light and US imaging methods could overcome the limitation of optical imaging (shallow penetration depth) and US imaging (possible misdiagnosis from the presence of gas bubbles), making PA imaging an effective tool for the visualization of tumour vasculature, microstructure and various tumour therapeutic process [129–132]. Jun et al. incorporated FA-coated chitosan onto graphene oxide (termed FA-CS-GO) through hydrogen bonding and electrostatic interaction and disclosed the ability of the nano assembly for the PA imaging of tumour photothermal therapy (PTT) (Fig. 4c) [83]. The FA-CS-GO effectively accumulated around the tumour and revealed a significantly amplified PA signal expressing a clear outline of tumour microstructure in the tumour-

bearing nude mice model (Fig. 4d). In contrast, only the major blood vessels could be observed before the injection of FA-CS-GO (Fig. 4e), indicating the performance of the as-developed nanoassemblies for enhanced PA imaging of tumours. Intriguingly, the intravenous injection of FA-CS-GO into tumour-bearing nude mice for PTT successfully eliminated the tumours, with no trace of recurrence within 20 days. A nano system with US and PA dual-imaging modality was recently developed [84]. The as-prepared MB comprises a porphyrin-lipid-based shell around a PFC gas bubble. Upon US irradiation, MB imploded and formed porphyrin-based NPs, where the encapsulated gas secured US imaging. At the same time, porphyrin gives rise to PA imaging. US-facilitated conversion of MB to NPs and the subsequent accumulation of porphyrin NPs in tumours were testified via PA imaging of KB xenograft-bearing mice.

### 3.2. Neurodegenerative diseases

Neurodegenerative disease is one of the notorious diseases to aged individuals worldwide, obtruding heavy economic and emotional

burdens to patients and their families. Neurodegeneration results from various complex reactions, such as amyloid protein aggregation, oxidative stress, metal ion dyshomeostasis, neurotransmitter malfunction, membrane potential fluctuation, etc. [133]. Importantly, these dynamic pathophysiological features occur in the central nervous system (CNS), which is well barricaded by the BBB that denies the entrance of most drugs to the CNS. The use of focused ultrasound (FUS) coupled with MBs for the transient opening of BBB appears to be an effective approach to increase the permeability of nanomaterials or drugs across BBB. The FUS-induced temporal BBB opening may be attributed to the vessel wall displacement resulting from the continuous compression and rarefaction of MBs [134]. To date, MB has been widely explored to be included in the nanomaterial formulations for BBB penetration. Liu et al. embedded quercetin-modified sulphur NPs (Qc@SNPs) on the shell of poly(α-cyanoacrylate n-butyl acrylate)-based MBs (denoted as Qc@SNPs-MB) for the treatment of Alzheimer's disease (AD) [85]. The Qc@SNPs-MB was destroyed upon US irradiation, leading to the opening of BBB and the release of Qc@SNPs to enter the CNS (Fig. 5a and b).

The formulation enabled a 5-fold better crossing efficiency than the endocytosis method and reduced neuronal apoptosis, amyloid protein aggregation, neuroinflammation, oxidative stress, and calcium dyshomeostasis due to Qc@SNPs. Additionally, the Morris water maze test revealed an improved learning and memory behaviour of AD mice compared to that of wild type (WT) control mice, reflecting the effectiveness of FUS + Qc@SNPs-MB for brain-targeted drug delivery (Fig. 5c). Lin et al. also utilized US-induced MB disruption to improve the delivery of neurotrophic factors (NFs) gene for Parkinson's disease management [86]. The authors first loaded glia cell line-derived NF (GDNF) and brain-derived NF (BDNF) in liposomes, followed by further encapsulating the gene liposomes in MBs to develop a novel gene nanocarrier MB complex (LpDNA-MB). With the aid of FUS, LpDNA-MBs effectively penetrated BBB and delivered NFs to the brain, reducing the

calcium expression, restoring normal dopamine secretion and rescuing the dopaminergic neuronal loss in 1-methyl-4-phenyl-1,2,3,6-tetrahydropyridine (MPTP)-treated PD mice models. The developed LpDNA-MBs in the preliminary study was, however, lacked the ability for specific targeting of disordered neurons. Thus, the further integration of ligands targeting the pathological factors of neurodegeneration to the nanocarrier is believed to enhance its promises for neuroprotective therapy against neurodegenerative diseases. Epilepsy is a neurological disorder characterized by recurrent spontaneous seizures due to abnormalities in neuronal membrane potential, reported affecting around 1% of the human population worldwide [135]. Airan et al. achieved the successful modulation of epileptic condition *in vivo* based on FUS gated propofol release from nanoemulsions [87]. The nanoemulsion was formed using propofol-loaded polymeric micelles as the emulsifier to stabilize PFC5. When the nanoemulsions were sonicated at high frequency (1 MHz), PFC5 with a low boiling point (28 °C) undergoes a phase transition, releasing the anaesthetic propofol to combat epileptic seizures. The introduction of the as-prepared nanoformulation to acute epileptic mice with US treatment yielded the silencing of seizure activity without causing a harmful effect to the brain, indicating the promising potential of the as-developed strategy for the treatment of epilepsy.

SDT has also been attempted for the treatment of neurodegenerative disease. Specifically, Xu et al. designed a US-assisted multifunctional NP-containing protoporphyrin IX (PX) for the inhibition of tau phosphorylation and beta-amyloid (Aβ) protein aggregation [88]. The nanomaterial comprises PX-loaded oxidized mesoporous carbon nanosphere (OMCN) coated with PEG (for colloidal stability and functionalized with rabies virus glycoprotein (RVG) peptide (brain-targeting peptide)). With the assistance of the RVG peptide, the nanospheres (PX@OMCN@PEG(OP)@RVG) target n-acetylcholine receptors widely available on brain parenchyma cells and BBB to enable BBB penetration. After internalising PX@OP@RVGs in the brain, US was applied to
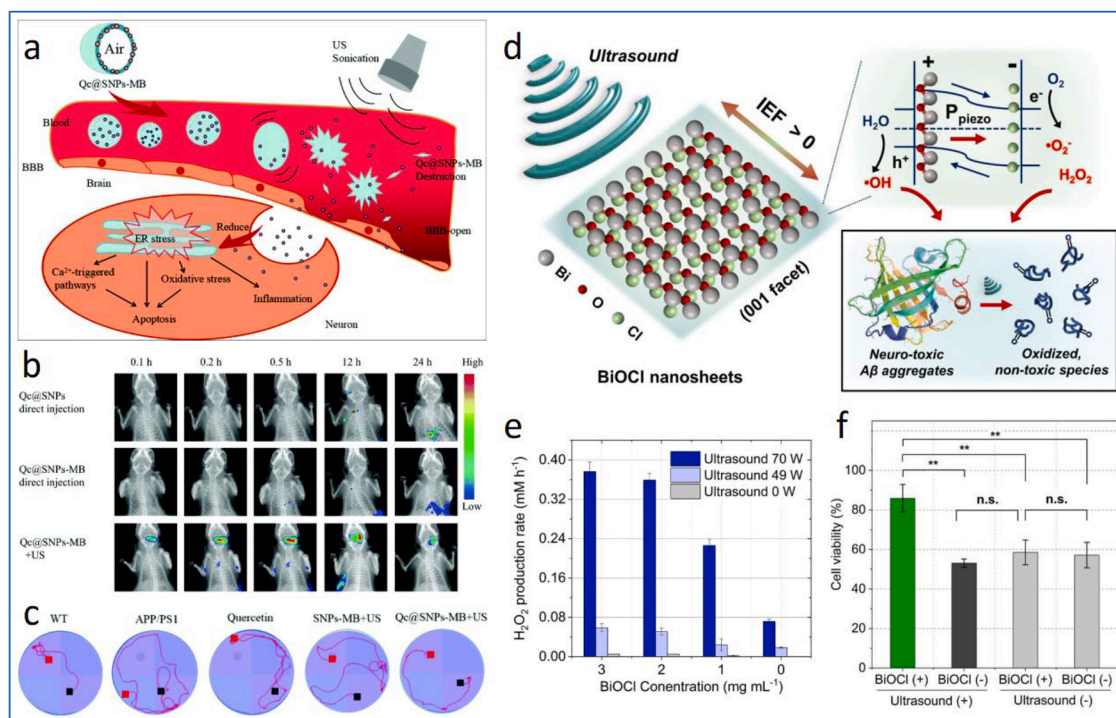
Fig. 5. Schematic representation of the delivery and US-assisted implosion of Qc@SNPs-MB to open the BBB and increase the permeability of Qc@SNPs into CNS, where the QC@SNPs are then internalized into neurons to relieve oxidative stress, inflammation, Ca²⁺ dyshomeostasis and cell apoptosis. (b) In vivo fluorescence images of mice subjected to Qc@SNPs, Qc@SNPs-MB and Qc@SNPs + US. (c) Water maze test of WT and AD mice subjected to different formulations. (d) Schematic diagram of piezoelectric dissociation of Aβ aggregates on the surface of BiOCl nanosheets under US irradiation. (e) H_2O_2 production rate under different BiOCl concentrations and US powers. (f) Cell viability of N2a cells incubated with Aβ aggregates after subjecting to different treatment groups without/with BiOCl and US sonication. Reprinted from [85,89] with permission from the Royal Society of Chemistry and Elsevier.

initiate SDT, which reduces amyloid aggregations and silences the glycogen synthase kinase-3 beta (GSK3β)-mediated tau phosphorylation in AD mice models. Similarly, Jang et al. demonstrated piezoelectric materials for US-triggered dissociation of Aβ [89]. The bismuth oxychloride (BiOCl) nanosheet containing $[Bi_2O_2]^{2+}$ and Cl^- layered

structure with $\langle 001 \rangle$ facet was used as the piezoelectric material, whereby the internal electric field along $\langle 001 \rangle$ was found to be responsible for the spatial separation transport of carriers in the nanosheet [136,137]. Upon US stimulation, BiOCl experienced a change in the local dipole moment, leading to piezoelectric polarization that
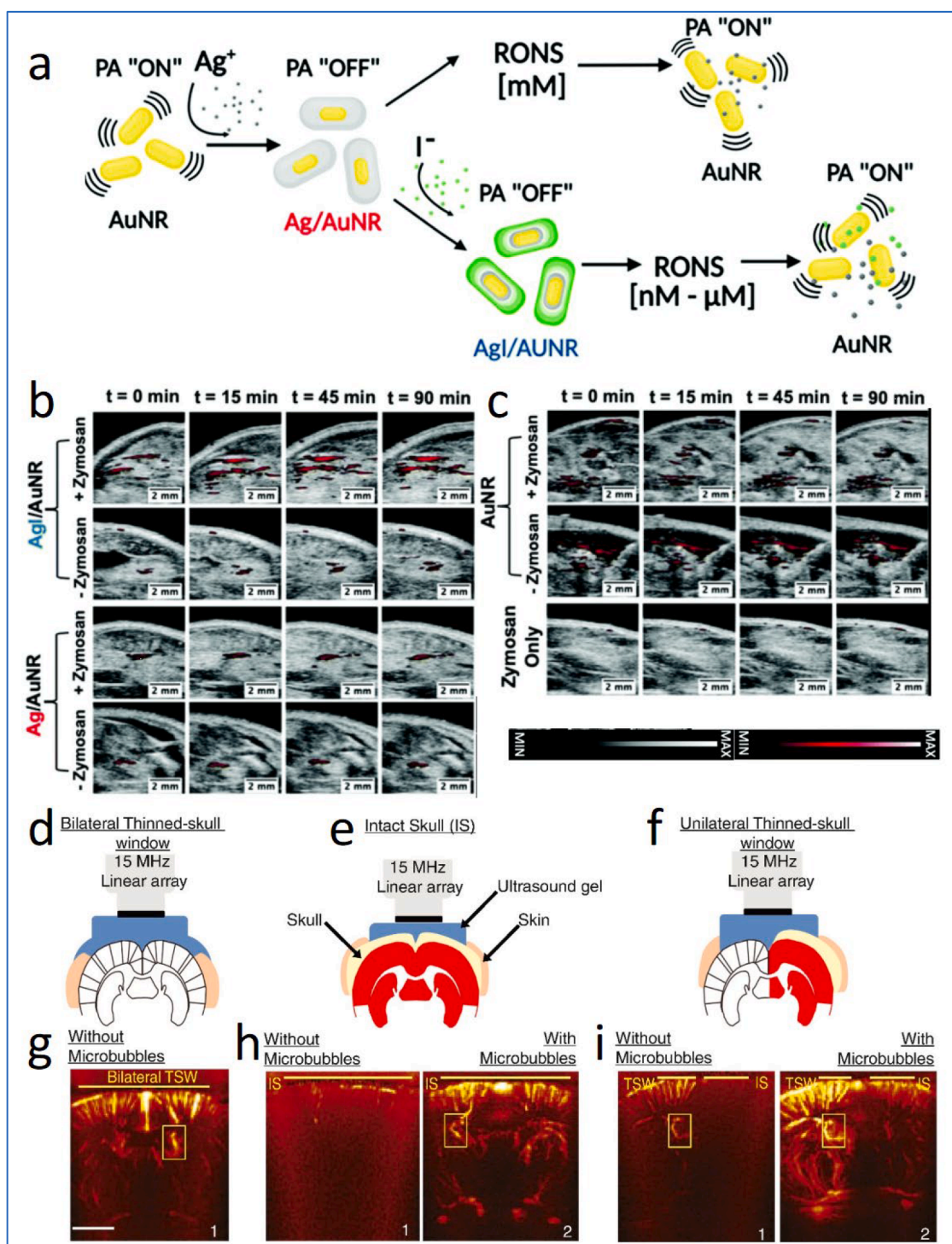
Fig. 6. (a) Schematic diagram showing the synthesis and functionalities of iodide-doped Ag/AuNR for RONS detection. (b and c) PA images expressing the oxidative stress in murine models using Zymosan as the ROS generating agent. The PA signal is acquired at 680 nm at different time intervals. Schematic illustration of high-resolution ultrafast Doppler imaging of the brain vasculature of mice through (d) bilateral thinned-skull window (TSW), (e) intact skull (IS), and (f) unilateral thinned-skull window (with both TSW and IS). Mice brain vascular images under (g) bilateral TSW without MBs (h) IS without/with MBs and (i) unilateral TSW without/with MBs. Yellow boxes in g-h indicate the fUS signal in the choroid plexus of the lateral ventricle, allowing the correct setup of the US probe. All scale bar = 2 mm. Reprinted from [90,92] with permission from the Royal Society of Chemistry and Elsevier. (For interpretation of the references to colour in this figure legend, the reader is referred to the web version of this article.)

generated an internal electric field to separate electron hole pairs of the BiOCl nanosheets to trigger the conversion of water molecules, O_2 and H_2O_2 into ROS [138], thereby dissociating Aβ aggregates (Fig. 5d-f). The ex vivo studies on AD mice models revealed the dramatically reduced Aβ plaques (by nearly 5-folds) after US treatment, suggesting the potential of the piezoelectric nanomaterials for SDT-based AD management. Although the studies presented above inhibited protein aggregations in AD mice using ROS, it should be advised that ROS is also the main cause of oxidative stress, and their excessive presence may stimulate the β-site amyloid precursor protein cleaving enzyme 1 (BACE1) expressions further to promote the aggregation of Aβ protein [139]. Therefore, ROS generation techniques should be carefully monitored when dealing with neurodegenerative diseases to avoid the undesired development and progression of neurodegenerative processes.

Diagnosis and monitoring of neurodegenerative progression are important to help to determine the right treatment course for a patient. Lately, US and PA imaging revealed substantial promises to detect neurodegenerative symptoms [140]. The building of oxidative stress (RONS overproduction) is one of the typical features in neurodegenerative diseases that are harmful to neurons, and nanomaterial delivery for oxidative stress alleviation has been a widely explored strategy to manage neurodegenerative disorder [133]. Mantri et al. demonstrated the use of iodide doped and silver (Ag)-coated gold (Au) nanorods as the ROS and reactive nitrogen species (RNS) sensor (RONS) [90]. Ag-coated Au nanorod (Ag-AuNR) functions through the oxidation of Ag ions by RONS, thereby reactivating the temporarily censored NIR resonance of Au (Fig. 6a). The resultant PA signal indicates the amount of Ag^+ released, which is directly proportional to the RONS content (Fig. 6b and c). Iodide doping was introduced to reduce the standard reduction potential of Ag to match the oxidation potential of RONS. The iodide modification provided the Ag-AuNR system with a 45-fold faster Ag etching and the improved H_2O_2 (representing ROS) and $ONOO^-$ (representing RNS) sensitivity by 1000- and 100000-fold, respectively, as compared to non-iodide doped Ag-AuNR. Besides oxidative damage, disordered neurons are also associated with mitochondrial dysfunction and neuroinflammation, making them the hallmarks for detecting neurodegenerative disorders. Chen et al. investigated a mitochondria-targeted probe termed TPP-HCy-BOH for fluorescence/PA dual-modal detection of H_2O_2 [91]. The nanoprobe consists of TPP for mitochondria targeting, boronic acid (BOH) for H_2O_2 recognition and hemocyanin (HCy) expressing fluorescence and PA signals under NIR exposure. The fluorescence and PA signals of TPP-HCy-BOH were at "offline" mode during the transportation as the optically tunable hydroxyl group of HCy was silenced by BOH. After TPP-mediated cellular internalization, the overexpressed H_2O_2 cleaves the BOH, thereby uncaging the hydroxyl group of HCy for intramolecular charge transfer responsible for switching on its fluorescence and PA signals. Using inflamed mice models, the TPP-HCy-BOH exhibited 2-fold higher H_2O_2 sensitivity and 30 min longer retention time than the control sample without TPP, suggesting the potential of the formulation in diagnosing mitochondria oxidative stress. Despite the beneficial outputs from the studies mentioned above, future investigation against neurodegeneration-associated animal models will be needed to verify the applicability of the as-synthesized TPP-HCy-BOH for diagnosing and treating CNS diseases.

Assessment of cerebral vascular morphology is one of the key approaches to disclosing CNS abnormalities [94]. Recently, a very high frame rate of US imaging has shown highly sensitive mapping of cerebral blood volume and brain elasticity in small animals [141,142]. Such imaging, typically known as functional US (fUS), is noticed to be feasible to differentiate slow-moving blood (down to 1 mm/s) from surrounding tissue, which enabled the detection of blood flow changes even if the spatial resolution is insufficient to map the vessel [92,142]. However, the application of US on the brain remains limited owing to the presence of the skull that attenuates US wave and disturbs its performance to distinguish small changes in blood flow [143]. The sensitivity of brain US imaging could be enhanced following the injection of MBs to combat the attenuation of US waves by the skull. One of the earliest works was done by Errico and colleagues [92]. As observed in Fig. 6, the intact skull attenuated the US waves, almost completely hindering the mapping of the rat brain's blood vessels.

In contrast, the inclusion of MBs significantly compensates the US signal, thus favoring the successful mapping of rat brain vasculature up to a depth of 12.5 mm. Strikingly, the presence of MBs also allowed the measurement of hemodynamic changes in the rat brain, with a comparatively higher resolution than the conventional method (skull thinning) to overcome the US wave attenuation (Fig. 6d-i). More recently, Maresca et al. also introduced nanoscale GVs-derived from cyanobacteria to enhance the hemodynamic imaging by fUS in mice brains [93]. The use of GVs resulted in comparable amplification of the magnitude of the US signal while ensuring a substantially reduced signal fluctuation compared to MBs. Notwithstanding, the work is rather preliminary and did not evaluate the potential of GVs for neurodegenerative disease-targeted US imaging. Future research should focus on improving the specificity and circulation time of GV via surface modification. It should be mentioned that the employment of fUS imaging strategy with the presence of US contrast agents has also been extended to human trials [94,144]. However, only conventional unmodified contrast agents were utilized. This research gap should be addressed in the future by exploring engineered contrast agents to increase the specificity ad spatiotemporal resolution of US imaging.

3.3. Thrombosis

Thrombosis is the formation of a thrombus (blood clot) at the blood vessels, i.e., veins or arteries, and reduces the blood flow in the circulatory system. Thrombosis can be classified into two main types: (1) Arterial thrombosis, where a blood clot blocks an artery carrying blood from the heart to the rest of the body parts, often resulting in heart attack and ischemic stroke [145] (oxygen-rich blood does not supply to the brain). (2) Venous thrombosis, where a blood clot blocks a vein delivering blood back to the heart from the rest of the body, resulting in deep vein thrombosis and pulmonary embolism. Deep vein thrombosis usually develops in the legs when a blood clot in the major vein leads to pain and swelling and can lead to pulmonary embolism when the loosened blood clots travel to the lung, decreasing the amount of oxygen in the blood affect breathing capability. Thrombotic diseases such as ischemic stroke and pulmonary embolism can be life-threatening and require immediate treatment. Current thrombolysis therapy mostly involves administering anticoagulants to block the formation of new clots. The acute thrombotic disease has a narrow therapeutic window; for example, intravenous treatment by tissue plasminogen activators is required within 3 h after onset leading to morbidity and modality. Medication such as heparin injection can be used for immediate action (within hours) for life-threatening clotting. Usage of high dosed untargeted thrombolytic drugs can cause bleeding in unwanted sites [146] and increase the risk of bleeding such as prolonged nosebleed, coughing and vomit with blood etc. In emergency cases, clots can be removed surgically but increase recurrent risk.

Being classified as a serine protease found in epithelial cells, tissue plasminogen activator (tPA) (also known as rt-PA or t-PA) is one of the essential components on the dissolution of blood clots, with the role in activating plasminogen to form plasmin (enzyme) required to degrade fibrin (insoluble protein) that contributes to blood clotting [147]. tPA such as Alteplase, Reteplase and Tenecteplase, has been approved by US FDA [148] as the standard treatment for ischemic stroke. Due to the constraint in a limited therapeutic window, intensive studies have been carried out to prolong its half-life, enhance the targeted delivery via MBs or nanocarriers, and accelerate thrombolysis via mechanical aids such as ultrasound energy referred to as sonothrombolysis.

Uesugi et al. designed a novel nano-sized delivery system that initially suppressed the thrombolytic activity of tPA (monteplase) until

being exposed to ultrasound [95]. The tPA was loaded into cationised gelatin-coated with PEG chains and injected into rabbits with balloon injury of the right femoral artery. The tPA activity of these PEG-modified NPs was suppressed by 45%, with 100% recovery when exposed to ultrasound *in vitro*. It enhanced the half-life of tPA 3-times in the blood circulation due to gelatin complexation. Continuous ultrasound irradiation (1 MHz, 0.75 W/cm^2) was applied transcutaneously to the upper side of the thrombus for 60 min until successful thrombolysis was obtained. A complete recanalization has been reported with samples exposed to ultrasound.

On the other hand, recanalization in half of the animal samples injected free t-PA administration was reported. This finding suggested gelatin complexation could only suppress part of the tPA adverse effect, i.e., bleeding complication. Similar results were reported in a swine acute myocardial model [96]. The NPs comprised of tPA, basic gelatin and zinc ions suppressed tPA activity by 50% with full recovery by ultrasound *in vitro*. In vivo intravenous NPs injection shows approximately 25% of tPA activity and recovered completely under ultrasound application (1 MHz, 1 W/cm^2). Using the same dose of tPA, treatment without ultrasound recanalized only 1 of 10 swine while tPA-loaded NPs with ultrasound increased the recanalization rate to 9 of 10 swine within 30 min.

Another strategy with sonothrombolysis was developed using echogenic liposomes coupling with MBs. Echogenic liposomes (ELIP) are small artificial spherical vesicles composed of a phospholipid bilayer capable of reflecting diagnostic ultrasound waves [149]. Treatment with colour Doppler ultrasound has been reported to release a significant amount of tPA (p < 0.01) from ELIP [150]. Moreover, ELIP is advantageous in sonothrombolysis due to its follow-up echography (ultrasound imaging display can be used for process monitoring) in the whole process of thrombus evolution. Laing et al. reported *in vivo* complete recanalization in the aorta of rabbit after 15 min administration of tPA-loaded ELIP (alteplase) with exposure of 5.7 MHz pulsed Doppler ultrasound, 0.4 mechanical index (MI) [97]. They further compared the thrombolytic efficacy of tPA-loaded ELIP with different sonification protocols using the same rabbit model: free tPA alone [151] and free tPA co-administered with MBs [152-156] (DefinityR, an ultrasound contrast agent for cavity opacification). Among all ultrasound treatment groups, tPA-loaded ELIP were more efficacious than others, although statistically insignificant differences. Total recanalization was observed in all treatment groups at least once but not in control animals (empty ELIP with ultrasound). The mean time for total recanalization for all sonothrombolytic treatment groups was approximately 14 min (p > 0.05). Following conclusions were reported: (1) encapsulated tPA has similar *in vivo* thrombolytic efficacy to free tPA (2) recanalization rates are inconsistent without ultrasound treatment, and cavitation effects at MI = 0.4 contributed better to thrombolysis than the acoustically driven diffusion provided at MI = 0.2. They further suggested improved protocols to be investigated with repeat tPA-loaded ELIP dosage for higher reproducibility in arterial recanalization. Similarly, Hagisawa et al. developed a PFC gas-containing ELIP, coated with thrombus targeting Arg-Gly-Asp (RGD) peptides, loaded with tPA (monteplase) [98]. Low frequency ultrasound (27 kHz) with low intensity (1.4 W/cm^2) and high intensity (4 W/cm^2) respectively, was applied *in vivo* to iliofemoral arteries thrombosis rabbit with higher recanalization rate (9 out of 10 rabbits) compared to animals with non-targeted liposomes (2 out of 10 rabbits) and sole tPA treatment (4 out of 10 rabbits).

On the other hand, Victor et al. developed magnetically targeted MBs with sonothrombolysis treatment [99]. The porcine blood clots placed in a partially occluded middle cerebral artery was treated with tPA, magnetic MBs and pulsatile ultrasound (500 kHz, 2% duty cycle). The magnetic targeting was achieved with a single permanent magnet placed 45° below the clot. A three-fold increase in lysis rates was observed for the combination of US + tPA + MBs + magnet compared to US + tPA + MBs. A significant increase in acoustic emissions with US + tPA + MBs with magnet was reported over without a magnet, validating the

hypothesis; magnetic targeting enhances cavitation energy by increasing the concentration of cavitation nuclei. A positive correlation between acoustic emissions in the focal region and lysis rate in the range of 2–5 MHz has been reported. Clot debris produced by this method were all smaller than 10 μm (similar to the size of red blood cells), indicating a low risk for downstream embolism (blockage caused by a broken blood clot from another location).

Another thrombolytic drug, urokinase (UK), is more cost-efficient and commonly used in China, although it is less specific with a relatively low success rate. Hence, Liu et al. studied the efficacy of transcranial Doppler ultrasound (TCD) mediated UK thrombolysis, with the addition of sulphur hexafluoride MBs, in a rabbit model of middle cerebral artery occlusion [100]. Through diagnostic TCD monitoring, 2 MHz (output power < 750 mW) ultrasound was continuously transmitted to the intracranial blood vessels, exposing the thrombus surface to residual blood. Thrombolysis rate was accelerated with a higher recanalization rate and smaller infarct size in the MBs plus UK group (56.3%) compared to the only UK group (31.3%). The application of ultrasound to the brain can be controversial. The brain, especially the gray matter, is very sensitive to ultrasound and may show degenerative changes upon exposure [157]; moreover, few studies have reported ultrasound-assisted thrombolysis increase the possibility of intracranial haemorrhage [158]. However, others have reported skull penetration rate of TCD ultrasound energy is 10–30%. It usually focuses on the interface between the intracranial thrombus and its surrounding weak blood flow when the signal is low [159]. The low-intensity signal (2 MHz with output power < 750 mW) used by Liu et al. is safe and did not injure the blood–brain barrier [160,161]. The UK-induced thrombolysis rate depends on the drug concentration and contact surface with the thrombus. The pulsatile energy from ultrasound causes fragmentation of the MBs, inducing strong shear stress and damage to the surface of the clot. These damaged surfaces develop tear-like changes, increasing contact area and enhanced the thrombolytic treatment. Shorter duration and lesser drug dosage are required for treatment assisted with ultrasound-activated MBs. Similar studies using the combination of TCD and MBs have been reported by other research groups using tPA as the delivered drug. Molina et al. evaluated 111 patients with acute stroke attributable to middle cerebral artery (MCA) occlusion treated with intravenous tPA and reported better recanalization in galactose MBs combined with TCD and tPA (54.5%) compared to TCD and tPA alone (40.8%) [101]. Alexandrov et al. combined perflutren-lipid microspheres with TCD and tPA and reported a recanalization rate of 83%.

Moreover, the perflutren-lipid microspheres permeated beyond intracranial occlusions caused no increase in symptomatic intracranial haemorrhage after systemic thrombolysis [102]. The Culp and Flores group reported good efficacy in reducing infarct volume in an acute ischemic stroke rabbit model using only perflutren-lipid microspheres/ MBs and TCD and concluded the effectiveness of ultrasound plus microbubble treatment is the same as using tPA alone in treating ischemic stroke [63,64]. This study was limited in the absence of correlation between microscopic bleeding in rabbits and symptomatic human bleeding beyond 24 h. The inability to separate effects of MBs *in vivo* was well presented during *in vitro* testing. They suggested conducting a study on a more severe stroke model and long-term survival studies for three days involving imaging strategies to assess better the evolution of brain injury and the progression of intracranial haemorrhage.

Mu et al. initially explored the feasibility of combining UK and Arg-Gly-Asp-Ser (RGDS) onto the surface of a microbubble-based ultrasound contrast agent, SonoVue, in 2009 [103]. They reported the highest binding rate at 1:1 of UK /RGDS, where the contrast agent aggregated on the surface of the femoral arterial thrombus emitting fluorescence from the labelled UK-RGDS. Mu et al. concluded that the binding contrast agent with the UK has *in vitro* thrombolysis ability and *in vivo* thrombotargeting effect. The prepared RGDS-targeted MBs and diagnostic ultrasound were evaluated histologically in a rabbit model with platelet-

rich thrombi in the femoral artery [104]. Six randomized groups were studied: ultrasound alone (US); UK alone (UK); ultrasound plus non-targeted MBs (US + M); ultrasound plus RGDS targeted MBs (US + R); RGDS-targeted MBs plus UK (R + UK); ultrasound plus non-targeted MBs and UK (US + M + UK); and ultrasound plus RGDS-targeted MBs and UK (US + R + UK). The diagnostic ultrasound (3.5 MHz, 1.0 mechanical index) was applied transcutaneously over the thrombus for 30 min. The thrombolytic effect was evaluated based on the ultrasound thrombi detection, blood flow and histological observations. The experimental results showed recanalization only in groups with a combination of RGDS-targeted microbubble and UK (R + UK and US + R + UK) during 120 min after treatment (Fig. 7). The large and high-amplitude wave was observed in the two groups, with higher and larger resonance waves after ultrasound flashing in the US + R + UK groups. Complete recanalization was achieved in the US + R + UK group with negative staining in tissue factor (TF) and von Willebrand factor (vWF), indicating no re-assembling platelets after treatment.

In contrast, the R + UK group showed partial recanalization where the fibre proteins and platelets re-assembled after treatment resulting in re-occlusion (blood flow dropped significantly after peak value). TF and vWF stained negative in US + M + UK and US + R + UK groups, but positive in R + UK group suggested inhibition of expression by ultrasound. The studies demonstrated that diagnostic ultrasound alone is capable of destroying the fibre network structure. Not to mention its capability when combining with targeted MBs and UK: to promote the release of targeted MBs; invade the thrombus through cavitation and resonance effects; enhance the delivery of UK into the inner fibrin matrix; inhibit the expression of TF and vWF, and reduce the chances of re-occlusion.

Alternative to drug carriers and MBs, a relatively new therapy, ultrasound-assisted catheter-directed thrombolysis, has been reported by Mohan et al. [162]. In their studies, a commercially available EkoSonic Endovascular System, an ultrasound-assisted catheter device [163], was used to elute tPA (alteplase) to patients with acute pulmonary embolism. The deployment of a device (bilateral or unilateral), the dose of thrombolytic eluted and duration of thrombolysis were all recorded according to the patients' conditions. The fibrinogen levels were recorded every 6 h, and the administration of tPA was stopped once the fibrinogen was below 100 mg/dL. The treatment reduced the right ventricle systolic pressure by a mean of 14.5 mmHg. It reduced the Qanadli index (quantification of pulmonary vascular obstruction, the weighting factor of 0, 1, or 2 for no thrombus, partial thrombus, or total occlusion, respectively) by 15.4. None of the patients experienced major bleeding, moderate bleeding, or intracranial haemorrhage during the treatment.

3.4. Diabetes

Diabetes mellitus is a type of disorder commonly classified as type 1 diabetes and type 2 diabetes, both resulting in high blood sugar (glucose) levels referred to as hyperglycemia. Diabetes complications include cardiovascular disease such as heart attack and cause severe damage to major organs such as nerve, kidney, brain and eyes. Treatment with insulin to lower the blood glucose back to normal level are often administered through subcutaneous injection. Patients often require three shots per day after meals or more according to their blood glucose levels. The subcutaneous injection can be inefficiently limited by the high molecular weight of insulin and the small amount of injection. Multiple injections induce physical and mental pain and are often accompanied by the risk of infection, inflammation, and skin disorders such as lipoatrophy [164]. Transdermal drug delivery with ultrasound, known as sonophoresis, has been studied by researchers for non-invasive insulin treatment.

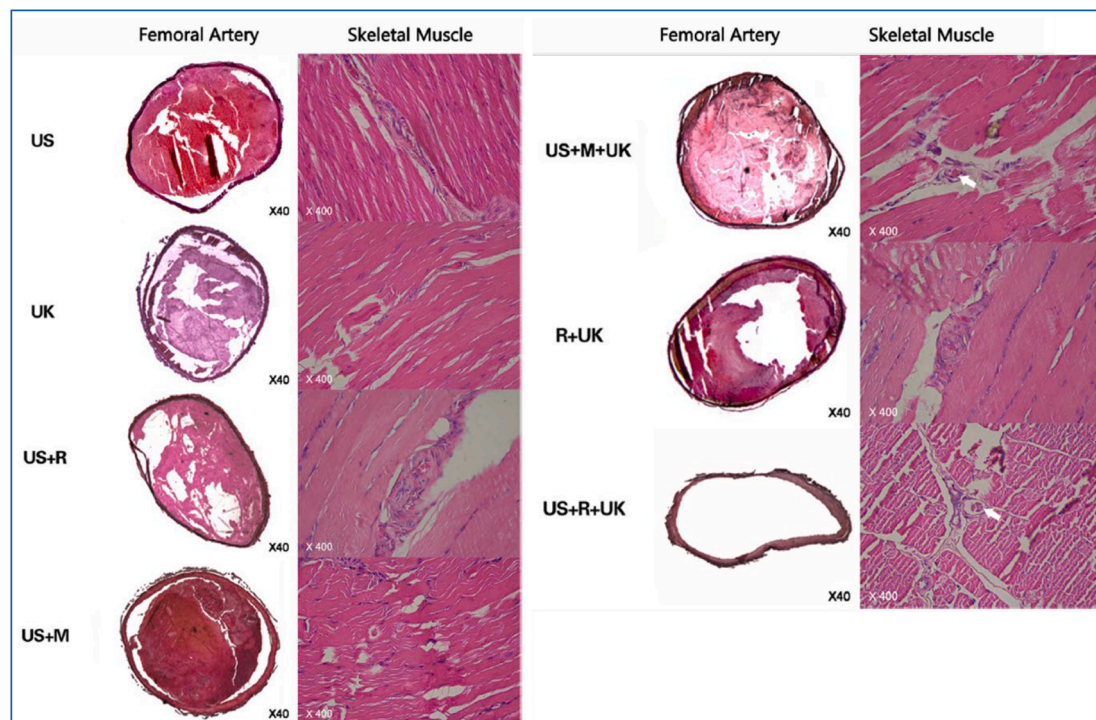Sonophoresis with commercially available hand-held ultrasound

Fig. 7. Rabbit femoral arteries stained by hematoxylin and eosin (x40). Histological examination showed the vessel was filled with thrombus and not completely dissolved for the group of US, UK, US + R, US + M, and US + M + UK; the platelets are granular and non-dense. The thrombi were partially dissolved in R + UK; no apparent boundaries and liquified platelets were observed. Complete recanalization was observed in the US + R + UK group, with no thrombi shown in the contralateral control arteries. The skeletal muscle staining (x400) show no micro thrombosis in the skeletal muscle for the US, UK, US + R, US + M, and R + UK groups. Micro thrombosis was present in the skeletal muscle microvessel for US + R + UK and US + M + UK groups. Reprinted from [104] with permission from Springer Nature.

devices have been reported at low frequency (20–100 kHz), moderate energy (0–3 W/cm^2), and short exposure time (5 min) [165]. Tachibana demonstrated insulin delivery to Alloxan-Diabetic rabbits via attached ultrasound on a concealed drug reservoir directly onto the skin [166]. The observed results demonstrate glucose level of the rabbits decreased to a minimum of 58.8 ± 13.4% at 3.5 h with low frequency (105 kHz) of ultrasound exposure. Interestingly, blood glucose levels continued to decrease after ultrasound and insulin exposure were stopped and gradually returned to the initial level at 6.5 h. Similar results have been reported by other scientists [167], where they speculate the accumulation of insulin in the stratum corneum (outer layer of skin, epidermis) and slow washout at the dermo-epidermal junction resulting in the delay of a systemic reaction. Although Brucks et al. reported no lag time in the human epidermis during ultrasound exposure, the results were not always reproducible [168]. The discrepancy between the plasma insulin concentration and blood glucose level were concluded by the short biological half-life and interanimal variation of metabolic breakdown of insulin. The contact skins were examined histologically and exhibited no inflammation and tissue destruction upon ultrasound exposure, further validating sonophoresis as an efficient non-invasive treatment, especially at low frequency.

Different researchers have reported similar transdermal insulin studies on hairless rat and *in vitro* human skin [169], where possible mechanisms induced by ultrasound were concluded: cavitation bubbles causing structural disorder of the stratum corneum lipids enhancing the skin permeability, thermal effects on the skin due to the absorbance of ultrasound energy increasing the skin permeability coefficient, and convective transport through hair follicles and sweat duct [170]. Recent studies show that acoustic cavitation plays a more significant role in sonophoresis than thermal effect and convective transport [44]. By combining ultrasound and NPs, Kost et al. implanted ultrasound-assisted polymeric materials incorporated with insulin into rats, showing convincing results of a 20-fold increased release rate in biodegradable polymer matrices such as polyanhydrides and 10-fold increased release rate in non-biodegradable ethylene/vinyl acetate copolymer. The release rate was proportional to ultrasound intensity, quantified by the exposure time. Their findings concluded cavitation effect plays a significant role in enhancing the polymer degradation while temperature and mixing remained relatively unimportant. The chemical integrity of the incorporated substances (20 mL solutions of p-Nitroaniline, insulin, bovine serum albumin, and p-amino hippuric acid) showed no differences upon ultrasound exposure, examined by HPLC and UV spectroscopy [105].

The administration of ultrasound-assisted drug carriers still requires subcutaneous injection. Fortunately, the polymer vesicles act as a protective layer to the drug and allow multiple releases from the same vesicle upon triggered with ultrasound to minimize the number of injections, as demonstrated by different researchers. Kwok et al. developed a self-assembled molecular structure, C12 methylene chains coating on co-polymer vesicle, consisting of 2-Hydroxyethyl methacrylate monomer (HEMA) and poly (ethylene glycol) dimethacrylate (PEGDMA), to allow controlled release of insulin [106]. The ultrasound irradiation transiently disrupted the orderly coated methylene chains and reassembled back to the impermeable barrier upon cessation. The diffusion of insulin from polymer was often reported to be difficult due to its larger protein molecules. PEG has been a recommended pore-forming agent incorporating insulin. It can create void spaces for unimpeded protein diffusion and insulin preferably partitioned in the microdomains, thus increasing the maximum drug loading [171,172].

Moreover, PEG can act as a solubilizer and preservative to prevent aggregation and degradation of insulin [173]. The *in vitro* results show instant peak release at low frequency (43 kHz) within the therapeutic range (4 U/h to 15 U/h) for 4–5 days; a similar trend was observed at 1.1 MHz. Interestingly, the trend shows a higher peak release on day 2. The hydrophobic coated film floated on the buffer during the first 24 h elution time, and water penetrates through and swells the core polymer,

causing insulin oversaturation of the interface. Acoustic cavitation and streaming were hypothesized to be the mechanism behind the transient distortion of the methylene chain. The suitability of poly(2-hydroxyethyl methacrylate) (pHEMA)/PEGDMA 0.4 K copolymer as an effective and sensitive insulin carrier with only minutes of ultrasound exposure was noted. In contrast, other reported polymer matrices required 1–2 h of ultrasound pre-treatment [174].

Instead of using only poly(lactic-co-glycolic acid) (PLGA) vesicles, Di and co-workers formulated an injectable three-dimensional cohesive gel-like nano-network consisting of alginate-coated PLGA (negative charge) and chitosan-coated PLGA (positive charge) (Fig. 8a) [107]. The NPs of opposite charges interact via electrostatic force to form a porous structure that enables drug release with near zero-order kinetics [175,176]. The nano-network had a shear-thinning effect when the FUS disrupted particle–particle interactions, promoting the release of insulin previously stored in the porous structure. The nano-network sensitively responded to 30-sec treatment, resulting in a 3.25-fold increase in the released insulin amount. The temperature change during the treatment shows insignificant rises (<2 °C) even at the most critical experimental condition: maximum treatment time (4 min), maximum input voltage (800 mVpp) and minimum pulse duration (20 sec), due to low acoustic absorption coefficient [177] of PBS solution. The significance of acoustic cavitation in enhancing release profiles was demonstrated when the released amount of insulin in the degassed buffer reduced up to 40% (without cavitation). It has been proposed that the enhancement of insulin release by cavitation can be related to the dissociation of nano-network due to the shock waves created by inertial cavitation and the rapid compression and expansion on the liquid, facilitating the rupture of polymer chains of PLGA, both triggering the release of insulin upon ultrasound exposure. Moreover, the collapse of cavitation bubbles creates perturbations in the surrounding liquid of the nano-network, increasing water penetration into the polymeric matrix. The acoustic streaming effect creates a gentle stirring force, facilitating the transport of insulin from the core [61].

The *in vivo* release profile in the streptozotocin (STZ)-induced type 1 mice was reported continuously up to day 10 (injection day is noted as day 0) with 30 sec of FUS treatment on days 2, 4, 7 and 10 (Fig. 8b). The blood glucose level declined immediately upon exposure and gradually reached the normoglycemia range (<200 mg/dL) an hour after the exposure; correspondingly, the significant increase of human plasma insulin was detected 30 min after the FUS trigger. Similar reductions upon trigger were observed in the remaining days, indicating practicability of long-term administration. The maximum reduced blood glucose level progressively decreases due to the depletion of encapsulated insulin, which could be overcome by optimizing the administration time, FUS power and pulse duration.

Di et al. conducted another similar study with insulin-loaded PLGA nanocapsules encapsulated by chitosan microgels [108]. The pulsatile release profile improved significantly with the newly developed system. Even after the sixth FUS activation, the *in vivo* blood glucose level was reduced to near 200 mg/dL. In contrast, in the previous study with nano-network, the amount of insulin released was already near exhaustion at the third FUS activation. The authors explained that the improved performance of microgels was due to the temporary storage of insulin in the microgel, thereby allowing the encapsulated insulin to diffuse passively in the nanocapsules and "recharge" the system before the next FUS treatment. The improved performance shows encouraging results to long-term sustained release with ultrasound therapeutics (Fig. 8c and d). The histological examination of the FUS exposed skin revealed no difference after multiple cycles of treatment. However, the injection site's position can be distinguished as a visible "bump". In contrast to existing ultrasound-mediated drug carriers [175,178–180], which have short half-lives (range from min to h), the two systems developed by Di et al. lasted for a week. The *in-vivo* studies showed that injected nano-network remains cohesive without significant viscosity changes after repeated FUS exposure. Besides, the injected nano-network and microgel did not
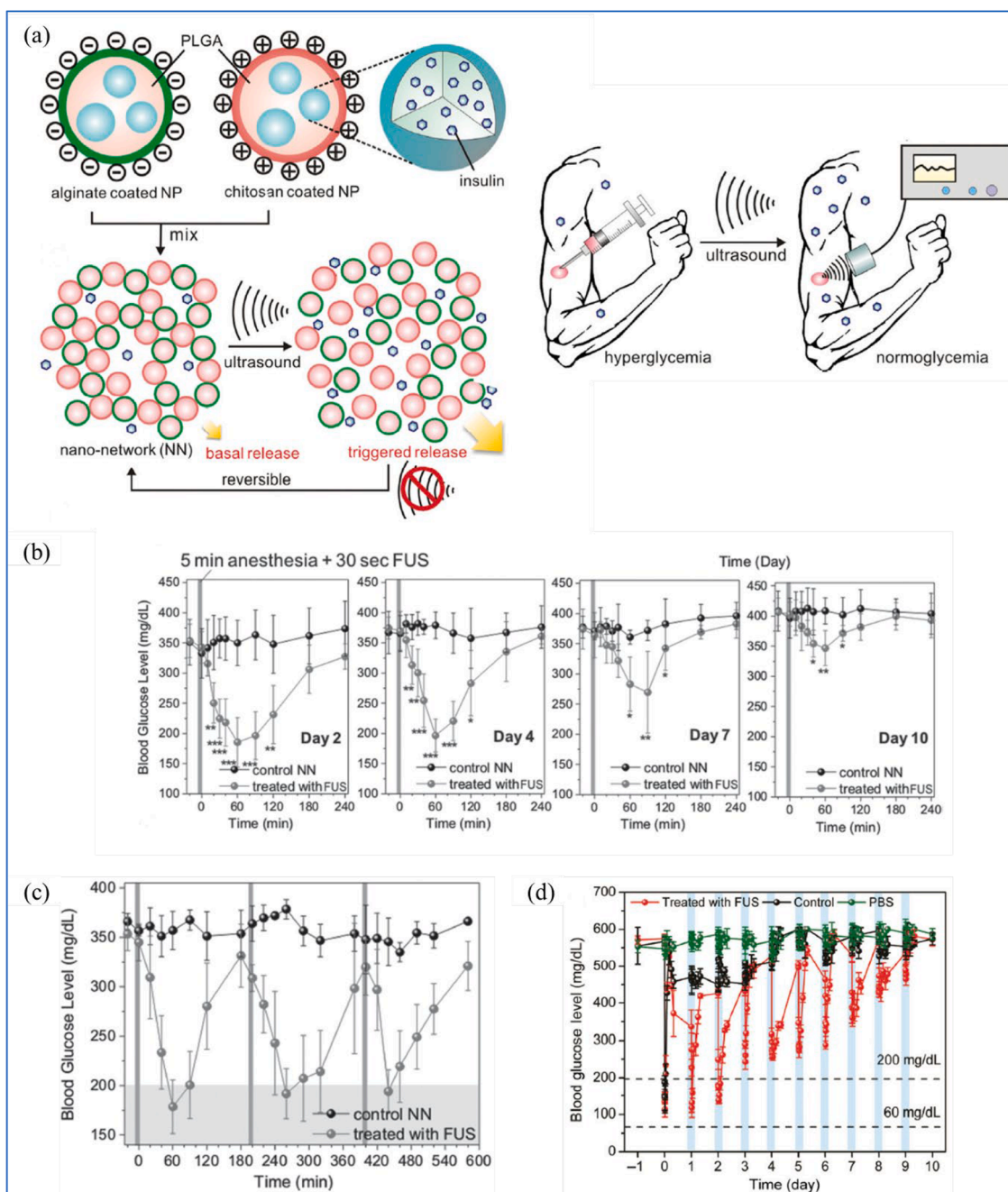
Fig. 8. (a) Schematic diagram of the focused ultrasound system (FUS)-mediated insulin delivery with nano-network formed by mixing oppositely charged NPs. The FUS triggers dissociation of nano-network to promote insulin release. (b) Subcutaneous injection of nano-network on day 0, FUS treatment was applied on day 2, day 4, day 7 and day 10 for 30 sec. The FUS treated mice and control group (without FUS) were recorded over time. (c) Three continuous FUS treatment cycles were applied on day 4 after the subcutaneous injection of nano-network into STZ-induced C57B6 diabetic mice. The blood glucose levels were recorded over time with solid lines indicating the administration window (5 min anaesthesia and 30-sec FUS treatment). (d) A continuous cycle of FUS treatment was applied once per day for ten days after the subcutaneous injection of chitosan microgel integrated with insulin-loaded PLGA nanocapsules into STZ-induced diabetic mice: one dose of microgel with FUS treatment (red line) or one dose of microgel without FUS treatment (black line) or PBS solution with FUS treatment (green line). (d). Reprinted from [107,108] with permission from Springer Nature and Wiley. (For interpretation of the references to colour in this figure legend, the reader is referred to the web version of this article.)

show cell-based cytotoxicity and was reported to be degraded completely after one month.

The function of destructed pancreatic beta cells (synthesize, store and release insulin) was restored via islet transplantation and promoted by UTMD-assisted gene delivery [181]. Shimoda et al. reported promising results in promoting the efficacy of human islets transplantation into livers of diabetic mice models via UTMD-assisted gene transfer and non-viral human vascular endothelial growth factor (VEGF). On day 30,

73% of mice in the VEGF group showed normal glucose levels, whereas transplantation without gene delivery (no-UTMD) only exhibited 13% restoration. Besides, the VEGF group demonstrated a significantly higher serum human insulin and C-peptide at day 32, indicating the improved efficacy [109]. Alternatively, from ultrasound-mediated polymer vesicles, Castellanos et al. reported direct ultrasound stimulation of insulin release from the pancreatic beta cells tested *in vitro*. A significant increase in insulin release has been reported at 24 ng/106

cells with 800 kHz ultrasound. The amount of insulin produced by ultrasound stimulation at this frequency is comparable to the response by natural secretagogue glucose under non-hyperglycemic conditions and maintaining the cell viability (from 97.8% to 95.8% cell viability, p > 0.05). The mechanism of the enhanced insulin secretion remains unknown and is to be studied [182]. Tania Singh et al. presented in the 177th Meeting of the Acoustical Society of America that measurable increases in mice's tested blood insulin levels were observed after the pancreas was exposed to the ultrasonic pulse. They hypothesized that the stimulation of the insulin release was caused by the calcium influx induced by the therapeutic ultrasound, applicable in type 2 diabetes where beta cells are still present. The therapeutic ultrasound shows promising results *in vitro* and *ex vivo*; however, it still poses uncertainties as a rise in insulin without a corresponding drop in glucose level during *in vivo* testing with mice was observed. Future studies suggested by them include modelling the T_{12} region of humans to determine appropriate acoustic window, pancreatic islets and whole pancreas to investigate the effects of therapeutic ultrasound on the exocrine pancreas. They also proposed to expand the studies to larger animals for further understanding.

3.5. Severe Acute Respiratory Syndrome Coronavirus 2 (COVID-19)

Coronavirus disease (COVID-19) infected by severe acute respiratory syndrome coronavirus 2 (SARS-CoV-2) has been defined as a pandemic by the World Health Organisation (WHO) due to its infectious outbreak globally. The sudden outbreak has infected over 206 million people globally, with 4.3 million deaths reported on 15th August 2021. Although the African Region reported a decrease in the case and death incidence, the data were incomplete and might be overestimated. Moreover, the Western Pacific and the Eastern Mediterranean Regions have reported the highest proportionate increases in death incidence of 23% and 15% respectively over the past seven days, not to mention the new variants developed from the current SARS-CoV-2 strain, which possesses new threats to the community [183]. Although the majority infected were able to self-recover from the mild to moderate respiratory illness; however, older people and those with underlying chronic disease are very likely to develop a serious illness that may lead to fatality. Pneumonia is one of the clinical manifestations of COVID-19, which occurs when the air sacs in one or both lungs are inflamed due to infections. The more severe case would lead to lasting damage in the lungs and other organs due to sepsis and acute respiratory distress syndrome (ARDS), a life-threatening lung injury [184,185].

Besides, patients infected were reported to have an increased risk of thromboembolic complications such as ischemic stroke [186,187]. The early infection stage of SARs-CoV-2 has been reported as the virus's incubation period, where infection may be asymptomatic. Patients show mild symptoms during the second stage, such as fever, dry cough, and tiredness; they can be diagnosed through a reverse-transcription polymerase chain reaction (RT-PCR) test through a nasopharyngeal swab in the pulmonary phase infection period [188]. At the third stage, patients exhibit severe symptoms leading to ARDS with a high viral load. The false-negative detection rate with RT-PCR has been reported to range from 5 to 40 % [189-191]. Hence chest computed tomography (CT) scan [192-195] and lung ultrasound (LUS) has been used to aid in diagnostic for asymptomatic patients (chest x-ray examination only reveal disease in the advanced stages).

The use of LUS has been established as a reliable diagnostic imaging tool to detect interstitial lung disease, subpleural consolidations, and ARDS from any etiologic cause, with high accuracy even in pregnancy [196-200] before the pandemic. Researchers have effectively reported the use of LUS [201-203] as the point of care diagnostic tool for early detection and monitoring COVID-19 patients with their advantages over chest radiograph and chest CT: (1) easily repeated at different time points without exposing patients to radiation; more sensitive than chest radiography in the diagnosis of the alveolar-interstitial syndrome; more

likely to detect lung lesions earlier when the lesions are located adjacent to the pleura, and reduce the exposure to healthcare workers (Fig. 9) [204]. Aiming for a global unified approach and communication between researchers, Soldati et al. have developed a standardized approach on the equipment and acquisition protocol with proposed a severity scoring system [205], which researchers later referenced in their studies [206-208]. Reynolds and co-workers reported the use of contrast-enhanced transcranial Doppler (TCD) to detect and quantify the MBs through injection of agitated saline into a central or peripheral venous catheter that appears in the cerebral circulation as a method to define the prevalence of intracardiac or intrapulmonary shunting in patients with COVID-19 [110]. The group reported that 83% of COVID-19 patients had TCD-detectable microbubble in the cerebral circulation, a higher prevalence than the ARDS patients (detected with contrast-enhanced transthoracic echocardiography). The number of MBs inversely correlated with oxygenation and lung compliance, suggesting it as a marker to define disease severity. The reported findings raised an important question: could intrapulmonary vasodilatation play a therapeutic role in managing hypoxemia associated with COVID-19? Archer and colleagues hypothesized impaired hypoxic pulmonary vasoconstriction as the reason for hypoxemia in COVID-19; suggesting medication drugs such as almitrine and indomethacin or methylene blue; to promote hypoxic vasoconstriction and inhibit endogenous vasodilator pathways, respectively [209]. These medications, however, are yet to be studied in COVID-19 pneumonia.

Therapeutic studies on hepatopulmonary syndrome (HPS), a pulmonary complication of liver disease characterized by intrapulmonary vasodilatation and impaired hypoxic pulmonary vasoconstriction resulting in hypoxemia, could provide useful insights: HPS response to 100% inspired oxygen can sometimes result in remarkably high Pa_{O_2}, reflecting the lack of associated alveolar damage seen in COVID-19 pneumonia [210]. Studies reported that medications such as almitrine shows no consistent benefit to HPS patients [211]. In contrast, therapies with inhaled pulmonary vasodilators such as inhaled nitric oxide improved oxygenation in HPS patients [212] and have been actively studied as a treatment for COVID-19. Although TCD was more sensitive than CT scan, it is less specific in distinguishing intracardiac from intrapulmonary shunting [213]. Hence, its advantage lies in the early diagnosis of COVID-19 patients to avoid overcrowded hospitals, especially in middle-income countries.

Mesenchymal Stem Cells (MSCs) and MSC-Derived Exosomes (MSC-EXO) presents the same therapeutic benefits [214] and has been reported to be able to repair lung damages resulting from viral infection due to their immunomodulatory functions [215]. COVID-19 patients with moderate to severe treatment with MSCs and MSC-EXO showed improved oxygenation, pulmonary function, higher levels of peripheral lymphocytes, and reduced cells that trigger cytokine storm [216]. Fonseca and group [111] have simulated the efficacy of ultrasound signals required to penetrate through layers of tissues reaching the alveoli to trigger the polymer-based encapsulated MBs [217] with MSC-EXO loading. The MBs remain in a state of dormancy until exposure to ultrasound signals, triggering the release of MSC-EXO for immediate treatment for lung damage and recovered patients who suffer from viral relapse infection: most patients recovered from COVID-19 suffered from lasting lung damage and were at risk of the second infection. Their simulation considers the attenuation and reflection of ultrasound waves, including denser lung characteristics due to the inflammation and mucus produced compared to healthy lungs that vary according to the severity of the infection. Better results are present in low frequency, i.e., 0.1 MHz regardless of the ultrasound intensity (94 mW/cm^2, 430 mW/cm^2, 720 mW/cm^2); four micro-bubbles ruptured and one oscillated. In comparison, most MBs only oscillate or show no excitation for frequency ranging from 0.3 to 5 MHz [111]. The simulation results have further validated the efficiency of low-frequency ultrasound in oscillating and vibrating MBs for controlled drug release.

Despite literature describing ultrasound and MBs for cargo delivery
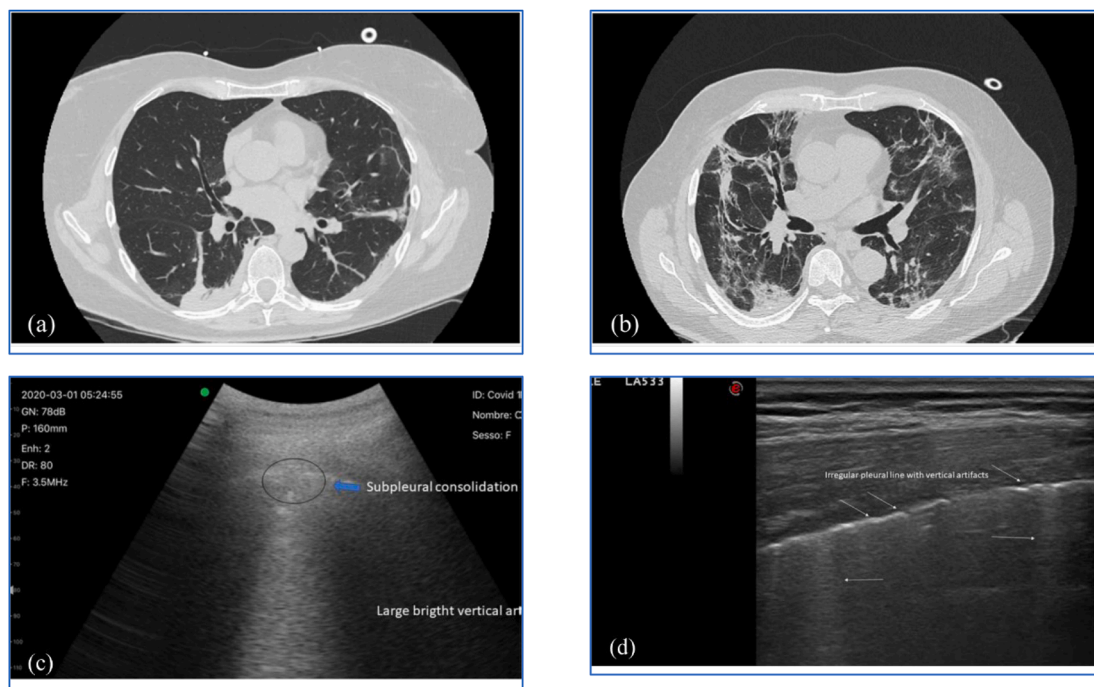
Fig. 9. Typical findings for patients with COVID-19 pneumonia. CT image of (a) peripheral ground glass lesion with consolidations and bronchiectasis and (b) consolidations and ground glass opacities associated with bronchiectasis and crazy paving pattern. LUS image of (c) subpleural consolidation and vertical artefact and (d) irregular pleural line with vertical artefacts. Reprinted from [204] with permission from the American Society of Tropical Medicine and Hygiene.

across the blood–brain barrier or enhancing drug delivery to targeted sites for diseases treatment as reported in the previous subsection, very few reports are related to the lung [25]. The early use of ultrasound in the lung mainly focused on studying pleural disease rather than lung tissue due to the scattering soundwaves in the air-filled lung tissue. Studies suggested thoracic ultrasound coupling with MBs are the ideal treatment for lung injury or ARDS as ultrasound waves can selectively penetrate to the most injured lung regions as fluid leaks into the alveoli, causing air loss in the lung [218]. The amount of ultrasound penetration can be quantitatively estimated with an acoustic impedance of lung tissue, air and blood and used to differentiate the injured fluid-filled lung regions and normal air-filled lung regions [219]. Ultrasound MBs mediated drug delivery can be potentially useful in treating COVID-19 patients, especially in targeting the injured pulmonary endothelium due to heterogeneity in lung damage that cannot be targeted by current treatments [25].

4. Conclusions and future perspectives

From its early employment as imaging tools to the current service to provide on-demand nanomaterials for drug delivery, US is serving as an efficient external force offering new possibilities for various biomedical applications. The unique capabilities of US waves could give rise to physicochemical changes in a local environment, thus allowing controlled manipulation of US-assisted nanomedicines for site-specific disease diagnosis and therapy. To date, numerous US-mediated techniques for disease management, including drug delivery, SDT, membrane sonoporation, US imaging and PA imaging, have been developed. For instance, US cavitation could generate thermal and mechanical energy to disarm a US-assisted nanocarrier to trigger the release of encapsulated drugs. Besides, sonoluminescence produced through US cavitation could excite the sonosensitizer to yield ROS for SDT. The incorporation of MBs was noticed to reduce the cavitation threshold and facilitate higher ROS generation. FUS also enables enhanced penetration of nanomaterials into disease or brain sites through sonoporation and BBB opening, respectively. Acoustic cavitation can temporarily improve

the permeability of the stratum corneum and enhance the transdermal drug delivery such as insulin to treat diabetic patients. Low-frequency US does not cause damage to the skin, and its incorporation with a multiple release drug delivery system can further reduce the physical suffering for such chronic disease. Moreover, the effect of US can trigger the release of thrombolytic drugs inhibited by nano-carriers and achieve targeted lysis to avoid haemorrhage in the unwanted sites.

For US imaging, which differentiates disease and healthy tissues based on the differences in the absorbance of US waves by various tissues, US signals could be improved with the utilization of MB and contrast agents. Therefore, MBs should be carefully engineered to take on several functionalities to improve their ability to produce images with higher resolution. Like its therapeutic counterpart, MB can be surface functionalised to gain disease-targeting properties, thereby increasing their accumulation at the disease sites for enhanced US imaging capabilities. Moreover, incorporating appropriate functions to the MB may also realize their application in US-imaging guided disease therapy, which would be promising since the US could induce non-invasive, cost-effective, portable and easy handling real-time imaging of disease lesions. Noteworthy, the (US and PA) dual imaging of disease microenvironment is also feasible [84], securing the possibility to obtain structural (based on US imaging), functional and molecular (based on PA imaging) information to produce better images to guide a drug delivery process [from light to sound].

Although recent examples revealed encouraging results of US-assisted nanomaterials for managing various diseases, the current tested disease models (*in vitro* cell line and *in vivo* animal models) are mostly associated with homogenous cell populations cultured for a relatively short time. In contrast, some diseases, such as cancers and neurodegenerative diseases, could take a long period to develop and establish their heterogeneous pathological microenvironment [220-223]. Hence, the models used to testify the US-assisted nanomaterials should be upgraded to mimic the clinical trial conditions, evaluating the ability of US-assisted systems in a more mature disease microenvironment. On the other hand, the thickness of the skull of small animals, which differs significantly from that of humans, maybe unsuitable for

examining their ability to attenuate US waves [140,143]. In addition, although human brain exposure to low-frequency US waves has been reported to be safe, the application is still controversial, especially on the sensitive grey matter, which may show degenerative changes [157].

Moreover, most experiments lack follow-up responsive studies as the animal models were euthanized for close examination of skin and arteries. These limitations could be overcome using either larger animal or artificial models. For example, some studies have simulated the efficacy of US penetration into the human body [224]; the findings can be incorporated with the organ-on-chip system to obtain more findings before stepping into a clinical trial. Upon the COVID-19 pandemic, researchers have developed an LUS protocol for more standard and accurate diagnostic. Studies have also shown the benefits of US in targeting the heterogeneity in lung damage [25], suggesting US coupling MBs as an ideal treatment for ARDS. Combining both diagnostic and therapeutic US would benefit future medical applications in monitoring the patients' progress while triggering the release of drugs for treatment at the same time. Overall, we anticipate that implementing the methods mentioned above will increase the practicality of US-assisted nanomaterials and pave the way for their further clinical translation in the future.

CRediT authorship contribution statement

Sze Shin Low: Conceptualization, Investigation, Writing – review & editing. **Chang Nong Lim:** Data curation, Writing – original draft. **Maxine Yew:** Methodology, Writing – original draft. **Wai Siong Chai:** Formal analysis, Validation. **Liang Ee Low:** Data curation, Conceptualization. **Sivakumar Manickam:** Writing – review & editing, Project administration. **Beng Ti Tey:** Methodology, Resources. **Pau Loke Show:** Supervision, Funding acquisition.

Declaration of Competing Interest

The authors declare that they have no known competing financial interests or personal relationships that could have appeared to influence the work reported in this paper.

Acknowledgements

References

[1] S. Senapati, A.K. Mahanta, S. Kumar, P. Maiti, Controlled drug delivery vehicles for cancer treatment and their performance, Signal Transduction and Targeted Therapy 3 (2018) 7.

[2] R.M.S. Sigrist, J. Liau, A.E. Kaffas, M.C. Chammas, J.K. Willmann, Ultrasound Elastography: Review of Techniques and Clinical Applications, Theranostics 7 (2017) 1303–1329.

[3] M. Gallo, L. Ferrara, D. Naviglio, Application of Ultrasound in Food Science and Technology: A Perspective, Foods 7 (2018) 164.

[4] Y. Meng, K. Hynynen, N. Lipsman, Applications of focused ultrasound in the brain: from thermoablation to drug delivery, Nature Reviews, Neurology 17 (2021) 7–22.

[5] Y. Tao, D. Li, W.S. Chai, P.L. Show, X. Yang, S. Manickam, G. Xie, Y. Han, Comparison between airborne ultrasound and contact ultrasound to intensify air drying of blackberry: Heat and mass transfer simulation, energy consumption and quality evaluation, Ultrason. Sonochem. 72 (2021), 105410.

[6] U.K. Zore, S.G. Yedire, N. Pandi, S. Manickam, S.H. Sonawane, A review on recent advances in hydrogen energy, fuel cell, biofuel and fuel refining via ultrasound process intensification, Ultrason. Sonochem. 73 (2021), 105536.

[7] J. Liu, F. Xu, J. Huang, J. Xu, Y. Liu, Y. Yao, M. Ao, A. Li, L. Hao, Y. Cao, Z. Hu, H. Ran, Z. Wang, P. Li, Low-intensity focused ultrasound (LIFU)-activated nanodroplets as a theranostic agent for noninvasive cancer molecular imaging and drug delivery, Biomaterials, Science 6 (2018) 2838–2849.

[8] D. Haemmerich, Non-invasive image-guided targeted drug delivery, Lancet Oncol. 19 (2018) 1000–1001.

[9] R. Geetha Bai, K. Muthoosamy, F.N. Shipton, S. Manickam, Acoustic cavitation induced generation of stabilizer-free, extremely stable reduced graphene oxide nanodispersion for efficient delivery of paclitaxel in cancer cells, Ultrason. Sonochem. 36 (2017) 129–138.

[10] P. Tharkar, R. Varanasi, W.S.F. Wong, C.T. Jin, W. Chrzanowski, Nano-Enhanced Drug Delivery and Therapeutic Ultrasound for Cancer Treatment and Beyond, Front. Bioeng. Biotechnol. 7 (2019).

[11] A. Jain, A. Tiwari, A. Verma, S.K. Jain, Ultrasound-based triggered drug delivery to tumors, Drug Delivery and Translational Research 8 (2018) 150–164.

[12] S. Sengupta, V.K. Balla, A review on the use of magnetic fields and ultrasound for non-invasive cancer treatment, J. Adv. Res. 14 (2018) 97–111.

[13] K. Entzian, A. Aigner, Drug Delivery by Ultrasound-Responsive Nanocarriers for Cancer Treatment, Pharmaceutics 13 (2021) 1135.

[14] D.B. Miller, J.P. O'Callaghan, New horizons for focused ultrasound (FUS) – therapeutic applications in neurodegenerative diseases, Metabolism 69 (2017) S3–S7.

[15] S. Masoudi Asil, J. Ahlawat, G. Guillama Barroso, M. Narayan, Nanomaterial based drug delivery systems for the treatment of neurodegenerative diseases, Biomaterials, Science 8 (2020) 4109–4128.

[16] Y. Zhang, J. Yu, A.R. Kahkoska, J. Wang, J.B. Buse, Z. Gu, Advances in transdermal insulin delivery, Adv. Drug Deliv. Rev. 139 (2019) 51–70.

[17] H. Ma, Z. Jiang, J. Xu, J. Liu, Z.-N. Guo, Targeted nano-delivery strategies for facilitating thrombolysis treatment in ischemic stroke, Drug Delivery 28 (2021) 357–371.

[18] B. Ihnatsenka, A. Boezaart, Ultrasound: Basic understanding and learning the language, International Journal of Shoulder Surgery 4 (2010) 55–62.

[19] M.K. Feldman, S. Katyal, M.S. Blackwood, US artifacts, Radiographics 29 (2009) 1179–1189.

[20] G. Soldati, R. Copetti, S. Sher, Sonographic interstitial syndrome: the sound of lung water, J. Ultrasound Med. 28 (2009) 163–174.

[21] Y. Watanabe, A. Aoi, S. Horie, N. Tomita, S. Mori, H. Morikawa, Y. Matsumura, G. Vassaux, T. Kodama, Low-intensity ultrasound and microbubbles enhance the antitumor effect of cisplatin, Cancer Sci. 99 (2008) 2525–2531.

[22] M. Ashokkumar, The characterization of acoustic cavitation bubbles – An overview, Ultrason. Sonochem. 18 (2011) 864–872.

[23] S. Mura, J. Nicolas, P. Couvreur, Stimuli-responsive nanocarriers for drug delivery, Nat. Mater. 12 (2013) 991–1003.

[24] J. Wischhusen, F. Padilla, Ultrasound-Targeted Microbubble Destruction (UTMD) for Localized Drug Delivery into Tumor Tissue, IRBM 40 (2019) 10–15.

[25] R. Sanwal, K. Joshi, M. Ditmans, S.S.H. Tsai, W.L. Lee, Ultrasound and Microbubbles for Targeted Drug Delivery to the Lung Endothelium in ARDS: Cellular Mechanisms and Therapeutic Opportunities, Biomedicines 9 (2021) 803.

[26] M.M. Forbes, R.L. Steinberg, W.D. O'Brien Jr., Frequency-dependent evaluation of the role of definity in producing sonoporation of Chinese hamster ovary cells, J. Ultrasound Med. 30 (2011) 61–69.

[27] I. Udroiu, Ultrasonic drug delivery in Oncology, JBUON 20 (2015) 381–390.

[28] S.B. Barnett, G.R. ter Haar, M.C. Ziskin, W.L. Nyborg, K. Maeda, J. Bang, Current status of research on biophysical effects of ultrasound, Ultrasound Med. Biol. 20 (1994) 205–218.

[29] J.M. Escoffre, J. Piron, A. Novell, A. Bouakaz, Doxorubicin delivery into tumor cells with ultrasound and microbubbles, Mol. Pharm. 8 (2011) 799–806.

[30] J. Wu, J. Pepe, M. Rincón, Sonoporation, anti-cancer drug and antibody delivery using ultrasound, Ultrasonics 44 (Suppl 1) (2006) e21–25.

[31] P.E. Huber, P. Pfisterer, In vitro and in vivo transfection of plasmid DNA in the Dunning prostate tumor R3327-AT1 is enhanced by focused ultrasound, Gene Ther. 7 (2000) 1516–1525.

[32] C. Pichon, K. Kaddur, P. Midoux, F. Tranquart, A. Bouakaz, Recent advances in gene delivery with ultrasound and microbubbles, J. Exp. Nanosci. 3 (2008) 17–40.

[33] A.P. McHale, J.F. Callan, N. Nomikou, C. Fowley, B. Callan, Sonodynamic Therapy: Concept, Mechanism and Application to Cancer Treatment, in: J.M. Escoffre, A. Bouakaz (Eds.) Therapeutic Ultrasound, 2016, pp. 429-450.

[34] N. Yumita, R. Nishigaki, K. Umemura, S. Umemura, Hematoporphyrin as a sensitizer of cell-damaging effect of ultrasound, Jpn. J. Cancer Res. 80 (1989) 219–222.

[35] S. Umemura, K. Kawabata, N. Sugita, K. Sasaki, N. Yumita, Sonodynamic approaches to tumor treatment, Int. Congr. Ser. 1274 (2004) 164–168.

[36] I. Rosenthal, J.Z. Sostaric, P. Riesz, Sonodynamic therapy–a review of the synergistic effects of drugs and ultrasound, Ultrason. Sonochem. 11 (2004) 349–363.

[37] D. Costley, C. Mc Ewan, C. Fowley, A.P. McHale, J. Atchison, N. Nomikou, J. F. Callan, Treating cancer with sonodynamic therapy: a review, Int. J. Hyperth. 31 (2015) 107–117.

[38] G.Y. Wan, Y. Liu, B.W. Chen, Y.Y. Liu, Y.S. Wang, N. Zhang, Recent advances of sonodynamic therapy in cancer treatment, Cancer Biology & Medicine 13 (2016) 325–338.

[39] A.K.W. Wood, C.M. Sehgal, A Review of Low-Intensity Ultrasound for Cancer Therapy, Ultrasound Med. Biol. 41 (2015) 905–928.

[40] G. Canavese, A. Ancona, L. Racca, M. Canta, B. Dumontel, F. Barbaresco, T. Limongi, V. Cauda, Nanoparticle-assisted ultrasound: A special focus on sonodynamic therapy against cancer, Chem. Eng. J. 340 (2018) 155–172.

[41] V. Misík, P. Riesz, Free radical intermediates in sonodynamic therapy, Ann. N. Y. Acad. Sci. 899 (2000) 335–348.

[42] A.P. Sviridov, L.A. Osminkina, A.L. Nikolaev, A.A. Kudryavtsev, A.N. Vasiliev, V. Y. Timoshenko, Lowering of the cavitation threshold in aqueous suspensions of porous silicon nanoparticles for sonodynamic therapy applications, Appl. Phys. Lett. 107 (2015), 123107.

[43] D. Bommannan, G.K. Menon, H. Okuyama, P.M. Elias, R.H. Guy, I. I. Sonophoresis, Examination of the mechanism(s) of ultrasound-enhanced transdermal drug delivery, Pharm. Res. 9 (1992) 1043–1047.

[44] S. Mitragotri, D.A. Edwards, D. Blankschtein, R. Langer, A mechanistic study of ultrasonically-enhanced transdermal drug delivery, J. Pharm. Sci. 84 (1995) 697–706.

[45] S. Mitragotri, J. Kost, Low-frequency sonophoresis: A noninvasive method of drug delivery and diagnostics, Biotechnol. Prog. 16 (2000) 488–492.

[46] H. Tang, S. Mitragotri, D. Blankschtein, R. Langer, Theoretical description of transdermal transport of hydrophilic permeants: application to low-frequency sonophoresis, J. Pharm. Sci. 90 (2001) 545–568.

[47] A. Tezel, A. Sens, S. Mitragotri, Investigations of the role of cavitation in low-frequency sonophoresis using acoustic spectroscopy, J. Pharm. Sci. 91 (2002) 444–453.

[48] T. Terahara, S. Mitragotri, J. Kost, R. Langer, Dependence of low-frequency sonophoresis on ultrasound parameters; distance of the horn and intensity, Int. J. Pharm. 235 (2002) 35–42.

[49] A. Tezel, A. Sens, J. Tuchscherer, S. Mitragotri, Frequency dependence of sonophoresis, Pharm. Res. 18 (2001) 1694–1700.

[50] G. Jones, F. Hunter, H.A. Hancock, A. Kapoor, M.J. Stone, B.J. Wood, J. Xie, M. R. Dreher, V. Frenkel, In vitro investigations into enhancement of tPA bioavailability in whole blood clots using pulsed-high intensity focused ultrasound exposures, IEEE Trans. Biomed. Eng. 57 (2010) 33–36.

[51] J.T. Sutton, N.M. Ivancevich, S.R. Perrin Jr., D.C. Vela, C.K. Holland, Clot retraction affects the extent of ultrasound-enhanced thrombolysis in an ex vivo porcine thrombosis model, Ultrasound Med. Biol. 39 (2013) 813–824.

[52] K.B. Bader, M.J. Gruber, C.K. Holland, Shaken and stirred: mechanisms of ultrasound-enhanced thrombolysis, Ultrasound Med. Biol. 41 (2015) 187–196.

[53] C. Acconcia, B.Y.C. Leung, K. Hynynen, D.E. Goertz, Interactions between ultrasound stimulated microbubbles and fibrin clots, Appl. Phys. Lett. 103 (2013), 053701.

[54] M. Nedelmann, C. Brandt, F. Schneider, B.M. Eicke, O. Kempski, F. Krummenauer, M. Dieterich, Ultrasound-Induced Blood Clot Dissolution without a Thrombolytic Drug Is More Effective with Lower Frequencies, Cerebrovascular Diseases 20 (2005) 18–22.

[55] Y.H. Chuang, P.W. Cheng, S.C. Chen, J.L. Ruan, P.C. Li, Effects of ultrasound-induced inertial cavitation on enzymatic thrombolysis, Ultrason. Imaging 32 (2010) 81–90.

[56] A.D. Maxwell, C.A. Cain, A.P. Duryea, L. Yuan, H.S. Gurm, Z. Xu, Noninvasive thrombolysis using pulsed ultrasound cavitation therapy - histotripsy, Ultrasound Med. Biol. 35 (2009) 1982–1994.

[57] X.B. Zhou, H. Qin, J. Li, B. Wang, C.B. Wang, Y.M. Liu, X.D. Jia, N. Shi, Platelet-targeted microbubbles inhibit re-occlusion after thrombolysis with transcutaneal ultrasound and microbubbles, Ultrasonics 51 (2011) 270–274.

[58] V. Suchkova, F.N. Siddiqi, E.L. Carstensen, D. Dalecki, S. Child, C.W. Francis, Enhancement of Fibrinolysis With 40-kHz Ultrasound, Circulation 98 (1998) 1030–1035.

[59] M. Fatar, M. Stroick, M. Griebe, A. Alonso, M.G. Hennerici, M. Daffertshofer, Brain Temperature During 340-kHz Pulsed Ultrasound Insonation, Stroke 37 (2006) 1883–1887.

[60] G. Bouchoux, R. Shivashankar, T.A. Abruzzo, C.K. Holland, In silico study of low-frequency transcranial ultrasound fields in acute ischemic stroke patients, Ultrasound Med. Biol. 40 (2014) 1154–1166.

[61] D.V. Sakharov, R.T. Hekkenberg, D.C. Rijken, Acceleration of fibrinolysis by high-frequency ultrasound: the contribution of acoustic streaming and temperature rise, Thromb Res 100 (2000) 333–340.

[62] A.F. Prokop, A. Soltani, R.A. Roy, Cavitational mechanisms in ultrasound-accelerated fibrinolysis, Ultrasound Med. Biol. 33 (2007) 924–933.

[63] W.C. Culp, R. Flores, A.T. Brown, J.D. Lowery, P.K. Roberson, L.J. Hennings, S. D. Woods, J.H. Hatton, B.C. Culp, R.D. Skinner, M.J. Borrelli, Successful microbubble sonothrombolysis without tissue-type plasminogen activator in a rabbit model of acute ischemic stroke, Stroke 42 (2011) 2280–2285.

[64] R. Flores, L.J. Hennings, J.D. Lowery, A.T. Brown, W.C. Culp, Microbubble-augmented ultrasound sonothrombolysis decreases intracranial hemorrhage in a rabbit model of acute ischemic stroke, Invest. Radiol. 46 (2011) 419–424.

[65] M. Ashokkumar, T.J. Mason, Sonochemistry, in: A. Seidel, M. Bickford (Eds.), Kirk-Othmer Encyclopedia of Chemical Technology, John Wiley and Sons, New York, 2007, pp. 1–34.

[66] A. Carovac, F. Smajlovic, D. Junuzovic, Application of ultrasound in medicine, Acta Informatica, Medica 19 (2011) 168–171.

[67] Z. Izadifar, P. Babyn, D. Chapman, Mechanical and Biological Effects of Ultrasound: A Review of Present Knowledge, Ultrasound Med. Biol. 43 (2017) 1085–1104.

[68] J.L. Paris, M. Manzano, M.V. Cabañas, M. Vallet-Regí, Mesoporous silica nanoparticles engineered for ultrasound-induced uptake by cancer cells, Nanoscale 10 (2018) 6402–6408.

[69] X. Song, L. Feng, C. Liang, K. Yang, Z. Liu, Ultrasound Triggered Tumor Oxygenation with Oxygen-Shuttle Nanoperfluorocarbon to Overcome Hypoxia-Associated Resistance in Cancer Therapies, Nano Lett. 16 (2016) 6145–6153.

[70] J. Wang, Y. Jiao, Y. Shao, Mesoporous Silica Nanoparticles for Dual-Mode Chemo-Sonodynamic Therapy by Low-Energy Ultrasound, Materials 11 (2018) 2041.

[71] C.-Y. Lin, M. Javadi, D.M. Belnap, J.R. Barrow, W.G. Pitt, Ultrasound sensitive eLiposomes containing doxorubicin for drug targeting therapy, Nanomedicine: Nanotechnology, Biology and Medicine 10 (2014) 67–76.

[72] N.-Q. Zhou, Z.-X. Fang, N. Huang, Y. Zuo, Y. Qiu, L.-J. Guo, P. Song, J. Xu, G.-R. Wan, X.-Q. Tian, Y.-L. Yin, P. Li, aFGF Targeted Mediated by Novel Nanoparticles-Microbubble Complex Combined With Ultrasound-Targeted Microbubble Destruction attenuates Doxorubicin-Induced Heart Failure via Anti-Apoptosis and Promoting Cardiac Angiogenesis, Front. Pharmacol. 12 (2021).

[73] X. Xiang, H. Pang, T. Ma, F. Du, L. Li, J. Huang, L. Ma, L. Qiu, Ultrasound targeted microbubble destruction combined with Fe-MOF based bio-/enzyme-mimics nanoparticles for treating of cancer, Journal of Nanobiotechnology 19 (2021) 92.

[74] P. Zhang, Z. Ren, Z. Chen, J. Zhu, J. Liang, R. Liao, J. Wen, Iron oxide nanoparticles as nanocarriers to improve chlorin e6-based sonosensitivity in sonodynamic therapy, Drug Des Devel Ther 12 (2018) 4207–4216.

[75] Y. Harada, K. Ogawa, Y. Irie, H. Endo, L.B. Feril, T. Uemura, K. Tachibana, Ultrasound activation of TiO2 in melanoma tumors, J. Control. Release 149 (2011) 190–195.

[76] Y. Cao, T. Wu, W. Dai, H. Dong, X. Zhang, TiO2 Nanosheets with the Au Nanocrystal-Decorated Edge for Mitochondria-Targeting Enhanced Sonodynamic Therapy, Chem. Mater. 31 (2019) 9105–9114.

[77] C.-C. Yang, C.-X. Wang, C.-Y. Kuan, C.-Y. Chi, C.-Y. Chen, Y.-Y. Lin, G.-S. Chen, C.-H. Hou, F.-H. Lin, Using C-doped TiO2 Nanoparticles as a Novel Sonosensitizer for Cancer Treatment, Antioxidants 9 (2020) 880.

[78] X. Wang, X. Wang, X. Zhong, G. Li, Z. Yang, Y. Gong, Z. Liu, L. Cheng, V-TiO2 nanospindles with regulating tumor microenvironment performance for enhanced sonodynamic cancer therapy, Appl. Phys. Rev. 7 (2020), 041411.

[79] Y. Li, H. An, X. Wang, P. Wang, F. Qu, Y. Jiao, K. Zhang, Q. Liu, Ultrasound-triggered release of sinoporphyrin sodium from liposome-microbubble complexes and its enhanced sonodynamic toxicity in breast cancer, Nano Res. 11 (2018) 1038–1056.

[80] R. Hou, X. Liang, X. Li, X. Zhang, X. Ma, F. Wang, In situ conversion of rose bengal microbubbles into nanoparticles for ultrasound imaging guided sonodynamic therapy with enhanced antitumor efficacy, Biomaterials, Science 8 (2020) 2526–2536.

[81] G. Wang, L. Song, X. Hou, S. Kala, K.F. Wong, L. Tang, Y. Dai, L. Sun, Surface-modified GVs as nanosized contrast agents for molecular ultrasound imaging of tumor, Biomaterials 236 (2020), 119803.

[82] Y. Liu, Y. Zhou, J. Xu, H. Luo, Y. Zhu, X. Zeng, F. Dong, Z. Wei, F. Yan, H. Zheng, Ultrasound molecular imaging-guided tumor gene therapy through dual-targeted cationic microbubbles, Biomaterials, Science 9 (2021) 2454–2466.

[83] S.W. Jun, P. Manivasagan, J. Kwon, V.T. Nguyen, S. Mondal, C.D. Ly, J. Lee, Y.-H. Kang, C.-S. Kim, J. Oh, Folic acid–conjugated chitosan-functionalized graphene oxide for highly efficient photoacoustic imaging-guided tumor-targeted photothermal therapy, Int. J. Biol. Macromol. 155 (2020) 961–971.

[84] E. Huynh, B.Y.C. Leung, B.L. Helfield, M. Shakiba, J.-A. Gandier, C.S. Jin, E. R. Master, B.C. Wilson, D.E. Goertz, G. Zheng, In situ conversion of porphyrin microbubbles to nanoparticles for multimodality imaging, Nat. Nanotechnol. 10 (2015) 325–332.

[85] Y. Liu, Y. Gong, W. Xie, A. Huang, X. Yuan, H. Zhou, X. Zhu, X. Chen, J. Liu, J. Liu, X. Qin, Microbubbles in combination with focused ultrasound for the delivery of quercetin-modified sulfur nanoparticles through the blood brain barrier into the brain parenchyma and relief of endoplasmic reticulum stress to treat Alzheimer's disease, Nanoscale 12 (2020) 6498–6511.

[86] C.-Y. Lin, Y.-C. Lin, C.-Y. Huang, S.-R. Wu, C.-M. Chen, H.-L. Liu, Ultrasound-responsive neurotrophic factor-loaded microbubble- liposome complex: Preclinical investigation for Parkinson's disease treatment, J. Control. Release 321 (2020) 519–528.

[87] R.D. Airan, R.A. Meyer, N.P.K. Ellens, K.R. Rhodes, K. Farahani, M.G. Pomper, S. D. Kadam, J.J. Green, Noninvasive Targeted Transcranial Neuromodulation via Focused Ultrasound Gated Drug Release from Nanoemulsions, Nano Lett. 17 (2017) 652–659.

[88] M. Xu, H. Zhou, Y. Liu, J. Sun, W. Xie, P. Zhao, J. Liu, Ultrasound-Excited Protoporphyrin IX-Modified Multifunctional Nanoparticles as a Strong Inhibitor of Tau Phosphorylation and β-Amyloid Aggregation, ACS Appl. Mater. Interfaces 10 (2018) 32965–32980.

[89] J. Jang, K. Kim, J. Yoon, C.B. Park, Piezoelectric materials for ultrasound-driven dissociation of Alzheimer's β-amyloid aggregate structure, Biomaterials 255 (2020) 120165.

[90] Y. Mantri, B. Davidi, J.E. Lemaster, A. Hariri, J.V. Jokerst, Iodide-doped precious metal nanoparticles: measuring oxidative stress in vivo via photoacoustic imaging, Nanoscale 12 (2020) 10511–10520.

[91] X. Chen, X. Ren, L. Zhang, Z. Liu, Z. Hai, Mitochondria-Targeted Fluorescent and Photoacoustic Imaging of Hydrogen Peroxide in Inflammation, Anal. Chem. 92 (2020) 14244–14250.

[92] C. Errico, B.-F. Osmanski, S. Pezet, O. Couture, Z. Lenkei, M. Tanter, Transcranial functional ultrasound imaging of the brain using microbubble-enhanced ultrasensitive Doppler, NeuroImage 124 (2016) 752–761.

[93] D. Maresca, T. Payen, A. Lee-Gosselin, B. Ling, D. Malounda, C. Demené, M. Tanter, M.G. Shapiro, Acoustic biomolecules enhance hemodynamic functional ultrasound imaging of neural activity, NeuroImage 209 (2020), 116467.

[94] C. Demené, J. Robin, A. Dizeux, B. Heiles, M. Pernot, M. Tanter, F. Perren, Transcranial ultrafast ultrasound localization microscopy of brain vasculature in patients, Nature, Biomed. Eng. 5 (2021) 219–228.

[95] Y. Uesugi, H. Kawata, J. Jo, Y. Saito, Y. Tabata, An ultrasound-responsive nano delivery system of tissue-type plasminogen activator for thrombolytic therapy, J. Control. Release 147 (2010) 269–277.

[96] H. Kawata, Y. Uesugi, T. Soeda, Y. Takemoto, J.H. Sung, K. Umaki, K. Kato, K. Ogiwara, K. Nogami, K. Ishigami, M. Horii, S. Uemura, M. Shima, Y. Tabata, Y. Saito, A new drug delivery system for intravenous coronary thrombolysis with

thrombus targeting and stealth activity recoverable by ultrasound, J. Am. Coll. Cardiol. 60 (2012) 2550–2557.

[97] S.T. Laing, M. Moody, B. Smulevitz, H. Kim, P. Kee, S. Huang, C.K. Holland, D. D. McPherson, Ultrasound-enhanced thrombolytic effect of tissue plasminogen activator-loaded echogenic liposomes in an in vivo rabbit aorta thrombus model–brief report, Arterioscler Thromb Vasc Biol 31 (2011) 1357–1359.

[98] K. Hagisawa, T. Nishioka, R. Suzuki, K. Maruyama, B. Takase, M. Ishihara, A. Kurita, N. Yoshimoto, Y. Nishida, K. Iida, H. Luo, R.J. Siegel, Thrombus-targeted perfluorocarbon-containing liposomal bubbles for enhancement of ultrasonic thrombolysis: in vitro and in vivo study, J. Thromb. Haemost. 11 (2013) 1565–1573.

[99] M. de Saint Victor, L.C. Barnsley, D. Carugo, J. Owen, C.C. Coussios, E. Stride, Sonothrombolysis with Magnetically Targeted Microbubbles, Ultrasound Med Biol 45 (2019) 1151–1163.

[100] W.S. Liu, Z.Z. Huang, X.W. Wang, J. Zhou, Effects of microbubbles on transcranial Doppler ultrasound-assisted intracranial urokinase thrombolysis, Thromb. Res. 130 (2012) 547–551.

[101] C.A. Molina, M. Ribo, M. Rubiera, J. Montaner, E. Santamarina, R. Delgado-Mederos, J.F. Arenillas, R. Huertas, F. Purroy, P. Delgado, J. Alvarez-Sabín, Microbubble Administration Accelerates Clot Lysis During Continuous 2-MHz Ultrasound Monitoring in Stroke Patients Treated With Intravenous Tissue Plasminogen Activator, Stroke 37 (2006) 425–429.

[102] A.V. Alexandrov, R. Mikulik, M. Ribo, V.K. Sharma, A.Y. Lao, G. Tsivgoulis, R. M. Sugg, A. Barreto, P. Sierzenski, M.D. Malkoff, J.C. Grotta, A pilot randomized clinical safety study of sonothrombolysis augmentation with ultrasound-activated perflutren-lipid microspheres for acute ischemic stroke, Stroke 39 (2008) 1464–1469.

[103] Y. Mu, L. Li, G. Ayoufu, Experimental study of the preparation of targeted microbubble contrast agents carrying urokinase and RGDS, Ultrasonics 49 (2009) 676–681.

[104] L. Guan, C. Wang, X. Yan, L. Liu, Y. Li, Y. Mu, A thrombolytic therapy using diagnostic ultrasound combined with RGDS-targeted microbubbles and urokinase in a rabbit model, Sci. Rep. 10 (2020) 12511.

[105] J. Kost, K. Leong, R. Langer, Ultrasound-enhanced polymer degradation and release of incorporated substances, Proc. Natl. Acad. Sci. 86 (1989) 7663.

[106] C.S. Kwok, P.D. Mourad, L.A. Crum, B.D. Ratner, Self-assembled molecular structures as ultrasonically-responsive barrier membranes for pulsatile drug delivery, J. Biomed. Mater. Res. 57 (2001) 151–164.

[107] J. Di, J. Price, X. Gu, X. Jiang, Y. Jing, Z. Gu, Ultrasound-triggered regulation of blood glucose levels using injectable nano-network, Adv Healthc Mater 3 (2014) 811–816.

[108] J. Di, J. Yu, Q. Wang, S. Yao, D. Suo, Y. Ye, M. Pless, Y. Zhu, Y. Jing, Z. Gu, Ultrasound-triggered noninvasive regulation of blood glucose levels using microgels integrated with insulin nanocapsules, Nano Res. 10 (2017) 1393–1402.

[109] M. Shimoda, S. Chen, H. Noguchi, S. Matsumoto, P.A. Grayburn, In vivo non-viral gene delivery of human vascular endothelial growth factor improves revascularisation and restoration of euglycaemia after human islet transplantation into mouse liver, Diabetologia 53 (2010) 1669–1679.

[110] A.S. Reynolds, A.G. Lee, J. Renz, K. DeSantis, J. Liang, C.A. Powell, C. E. Ventetuolo, H.D. Poor, Pulmonary Vascular Dilatation Detected by Automated Transcranial Doppler in COVID-19 Pneumonia, Am. J. Respir. Crit. Care Med. 202 (2020) 1037–1039.

[111] B. Fonseca, C. Fonseca, M. Barros, M. White, V. Abhyankar, D.A. Borkholder, S. Balasubramaniam, Ultrasound-based Control of Micro-Bubbles for Exosome Delivery in Treating COVID-19 Lung Damage, in, IEEE International Conference on Communications Workshops (ICC Workshops) 2021 (2021) 1–6.

[112] D. Hanahan, Robert A, Weinberg, Hallmarks of Cancer: The Next Generation, Cell 144 (2011) 646–674.

[113] P.N. Navya, A. Kaphle, S.P. Srinivas, S.K. Bhargava, V.M. Rotello, H.K. Daima, Current trends and challenges in cancer management and therapy using designer nanomaterials, Nano Convergence 6 (2019) 23.

[114] J.L. Paris, M.V. Cabañas, M. Manzano, M. Vallet-Regí, Polymer-Grafted Mesoporous Silica Nanoparticles as Ultrasound-Responsive Drug Carriers, ACS Nano 9 (2015) 11023–11033.

[115] A. Palani, H.-Y. Wu, C.-C. Ting, S. Vetrivel, K. Shanmugapriya, A.S.T. Chiang, H.-M. Kao, Rapid temperature-assisted sonochemical synthesis of mesoporous silica SBA-15, Microporous Mesoporous Mater. 131 (2010) 385–392.

[116] G. Song, C. Liang, X. Yi, Q. Zhao, L. Cheng, K. Yang, Z. Liu, Perfluorocarbon-Loaded Hollow Bi2Se3 Nanoparticles for Timely Supply of Oxygen under Near-Infrared Light to Enhance the Radiotherapy of Cancer, Adv. Mater. 28 (2016) 2716–2723.

[117] H. Lv, R. Tan, J. Liao, Z. Hao, X. Yang, Y. Liu, Y. Xia, Doxorubicin contributes to thrombus formation and vascular injury by interfering with platelet function, American Journal of Physiology-Heart and Circulatory, Physiology 319 (2020) H133–H143.

[118] G. Morciano, C. Giorgi, M. Bonora, S. Punzetti, R. Pavasini, M.R. Wieckowski, G. Campo, P. Pinton, Molecular identity of the mitochondrial permeability transition pore and its role in ischemia-reperfusion injury, J. Mol. Cell. Cardiol. 78 (2015) 142–153.

[119] M. Zhang, W.-Z. Yu, X.-T. Shen, Q. Xiang, J. Xu, J.-J. Yang, P.-P. Chen, Z.-L. Fan, J. Xiao, Y.-Z. Zhao, C.-T. Lu, Advanced Interfere Treatment of Diabetic Cardiomyopathy Rats by aFGF-Loaded Heparin-Modified Microbubbles and UTMD Technique, Cardiovasc. Drugs Ther. 30 (2016) 247–261.

[120] L. Serpe, F. Foglietta, R. Canaparo, Nanosonotechnology: the next challenge in cancer sonodynamic therapy, Nanotechnology Reviews 1 (2012) 173–182.

[121] X. Pang, C. Xu, Y. Jiang, Q. Xiao, A.W. Leung, Natural products in the discovery of novel sonosensitizers, Pharmacol. Ther. 162 (2016) 144–151.

[122] T. Yoshida, T. Kondo, R. Ogawa, L.B. Feril, Q.-L. Zhao, A. Watanabe, K. Tsukada, Combination of doxorubicin and low-intensity ultrasound causes a synergistic enhancement in cell killing and an additive enhancement in apoptosis induction in human lymphoma U937 cells, Cancer Chemother. Pharmacol. 61 (2008) 559–567.

[123] B. Liu, J. Wang, X. Wang, B.-M. Liu, Y.-M. Kong, D. Wang, S.-K. Xu, Spectrometric Studies on the Sonodynamic Damage of Protein in the Presence of Levofloxacin, Journal of Fluorescence 20 (2010) 985–992.

[124] H. Xu, X. Zhang, R. Han, P. Yang, H. Ma, Y. Song, Z. Lu, W. Yin, X. Wu, H. Wang, Nanoparticles in sonodynamic therapy: state of the art review, RSC Adv. 6 (2016) 50697–50705.

[125] T. Tuziuti, K. Yasui, M. Sivakumar, Y. Iida, N. Miyoshi, Correlation between Acoustic Cavitation Noise and Yield Enhancement of Sonochemical Reaction by Particle Addition, The Journal of Physical Chemistry A 109 (2005) 4869–4872.

[126] K. Ozawa, M. Emori, S. Yamamoto, R. Yukawa, S. Yamamoto, R. Hobara, K. Fujikawa, H. Sakama, I. Matsuda, Electron-Hole Recombination Time at TiO2 Single-Crystal Surfaces: Influence of Surface Band Bending, The Journal of Physical Chemistry Letters 5 (2014) 1953–1957.

[127] N. Nomikou, C. Fowley, N.M. Byrne, B. McCaughan, A.P. McHale, J.F. Callan, Microbubble–sonosensitiser conjugates as therapeutics in sonodynamic therapy, Chem. Commun. 48 (2012) 8332–8334.

[128] M. Xu, L.V. Wang, Photoacoustic imaging in biomedicine, Rev. Sci. Instrum. 77 (2006), 041101.

[129] S.C. Hester, M. Kuriakose, C.D. Nguyen, S. Mallidi, Role of Ultrasound and Photoacoustic Imaging in Photodynamic Therapy for Cancer, Photochem. Photobiol. 96 (2020) 260–279.

[130] G. Ku, X. Wang, X. Xie, G. Stoica, L.V. Wang, Imaging of tumor angiogenesis in rat brains in vivo by photoacoustic tomography, Appl. Opt. 44 (2005) 770–775.

[131] X. Wang, Y. Pang, G. Ku, X. Xie, G. Stoica, L.V. Wang, Noninvasive laser-induced photoacoustic tomography for structural and functional in vivo imaging of the brain, Nat. Biotechnol. 21 (2003) 803–806.

[132] S. Hu, K. Maslov, L.V. Wang, In vivo functional chronic imaging of a small animal model using optical-resolution photoacoustic microscopy, Med. Phys. 36 (2009) 2320–2323.

[133] L.E. Low, Q. Wang, Y. Chen, P. Lin, S. Yang, L. Gong, J. Lee, S.P. Siva, B.-H. Goh, F. Li, D. Ling, Microenvironment-tailored nanoassemblies for the diagnosis and therapy of neurodegenerative diseases, Nanoscale 13 (2021) 10197–10238.

[134] G. Leinenga, C. Langton, R. Nisbet, J. Götz, Ultrasound treatment of neurological diseases — current and emerging applications, Nature Reviews, Neurology 12 (2016) 161–174.

[135] D.J. Thurman, E. Beghi, C.E. Begley, A.T. Berg, J.R. Buchhalter, D. Ding, D. C. Hesdorffer, W.A. Hauser, L. Kazis, R. Kobau, D. Labiner, K. Liow, G. Logroscino, M.T. Medina, C.R. Newton, K. Parko, A. Paschal, P.-M. Preux, J. W. Sander, A. Selassie, W. Theodore, T. Tomson, S. Wiebe, f.t.I.C.o, Epidemiology, Standards for epidemiologic studies and surveillance of epilepsy, Epilepsia 52 (2011) 2–26.

[136] L. Zhang, W. Wang, S. Sun, D. Jiang, E. Gao, Selective transport of electron and hole among 001 and 110 facets of BiOCl for pure water splitting, Appl. Catal. B 162 (2015) 470–474.

[137] K.-L. Zhang, C.-M. Liu, F.-Q. Huang, C. Zheng, W.-D. Wang, Study of the electronic structure and photocatalytic activity of the BiOCl photocatalyst, Appl. Catal. B 68 (2006) 125–129.

[138] D. Shao, L. Zhang, S. Sun, W. Wang, Oxygen Reduction Reaction for Generating H2O2 through a Piezo-Catalytic Process over Bismuth Oxychloride, ChemSusChem 11 (2018) 527–531.

[139] J. Li, W. O, W. Li, Z.-G. Jiang, H.A. Ghanbari, Oxidative stress and neurodegenerative disorders, Int J Mol Sci 14 (2013) 24438–24475.

[140] Y. Tang X. Qian D.J. Lee Q. Zhou J. Yao From Light to Sound: Photoacoustic and Ultrasound Imaging in Fundamental Research of Alzheimer's Disease OBM Neurobiol 4 (2020) 10.21926/obm.neurobiol.2002056.

[141] E. Macé, G. Montaldo, I. Cohen, M. Baulac, M. Fink, M. Tanter, Functional ultrasound imaging of the brain, Nat. Methods 8 (2011) 662–664.

[142] E. Mace, G. Montaldo, B. Osmanski, I. Cohen, M. Fink, M. Tanter, Functional ultrasound imaging of the brain: theory and basic principles, IEEE Trans. Ultrason. Ferroelectr. Freq. Control 60 (2013) 492–506.

[143] G. Pinton, J.-F. Aubry, E. Bossy, M. Muller, M. Pernot, M. Tanter, Attenuation, scattering, and absorption of ultrasound in the skull bone, Med. Phys. 39 (2012) 299–307.

[144] S. Soloukey, A.J.P.E. Vincent, D.D. Satoer, F. Mastik, M. Smits, C.M.F. Dirven, C. Strydis, J.G. Bosch, A.F.W. van der Steen, C.I. De Zeeuw, S.K.E. Koekkoek, P. Kruizinga, Functional Ultrasound (fUS) During Awake Brain Surgery: The Clinical Potential of Intra-Operative Functional and Vascular Brain Mapping, Front. Neurosci. 13 (2020).

[145] D. Mozaffarian, E.J. Benjamin, A.S. Go, D.K. Arnett, M.J. Blaha, M. Cushman, S. R. Das, S.D. Ferranti, J.-P. Després, H.J. Fullerton, V.J. Howard, M.D. Huffman, C. R. Isasi, M.C. Jiménez, S.E. Judd, B.M. Kissela, J.H. Lichtman, L.D. Lisabeth, S. Liu, R.H. Mackey, D.J. Magid, D.K. McGuire, E.R. Mohler, C.S. Moy, P. Muntner, M.E. Mussolino, K. Nasir, R.W. Neumar, G. Nichol, L. Palaniappan, D. K. Pandey, M.J. Reeves, C.J. Rodriguez, W. Rosamond, P.D. Sorlie, J. Stein, A. Towfighi, T.N. Turan, S.S. Virani, D. Woo, R.W. Yeh, M.B. Turner, Heart Disease and Stroke Statistics—2016 Update, Circulation 133 (2016) e38–e360.

[146] T. Huang, N. Li, J. Gao, Recent strategies on targeted delivery of thrombolytics, Asian, J Pharm Sci 14 (2019) 233–247.

[147] T.N. Jilani, A.H. Siddiqui, Tissue Plasminogen Activator, in: StatPearls, StatPearls Publishing Copyright © 2021, StatPearls Publishing LLC., Treasure Island (FL), 2021.

[148] L.A. Tu, FDA Information on Medication Errors Involving Activase and TNKase, in: D.o.M.E.P.a. Analysis (Ed.), FDA, FDA News for Health Professional, 2015.

[149] K.D. Buchanan, S. Huang, H. Kim, R.C. Macdonald, D.D. McPherson, Echogenic liposome compositions for increased retention of ultrasound reflectivity at physiologic temperature, J. Pharm. Sci. 97 (2008) 2242–2249.

[150] C.K. Holland, D.D. McPherson, Echogenic liposomes for image-guided drug delivery, The Journal of the Acoustical Society of America 123 (2008) 3112.

[151] A.V. Alexandrov, C.A. Molina, J.C. Grotta, Z. Garami, S.R. Ford, J. Alvarez-Sabin, J. Montaner, M. Saqqur, A.M. Demchuk, L.A. Moyé, M.D. Hill, A.W. Wojner, Ultrasound-enhanced systemic thrombolysis for acute ischemic stroke, The New England Journal of Medicine 351 (2004) 2170–2178.

[152] A.T. Brown, R. Flores, E. Hamilton, P.K. Roberson, M.J. Borrelli, W.C. Culp, Microbubbles improve sonothrombolysis in vitro and decrease hemorrhage in vivo in a rabbit stroke model, Invest. Radiol. 46 (2011) 202–207.

[153] W.C. Culp, E. Erdem, P.K. Roberson, M.M. Husain, Microbubble potentiated ultrasound as a method of stroke therapy in a pig model: preliminary findings, J. Vasc. Interv. Radiol. 14 (2003) 1433–1436.

[154] W.C. Culp, T.R. Porter, J. Lowery, F. Xie, P.K. Roberson, L. Marky, Intracranial clot lysis with intravenous microbubbles and transcranial ultrasound in swine, Stroke 35 (2004) 2407–2411.

[155] F. Xie, J.M. Tsutsui, J. Lof, E.C. Unger, J. Johanning, W.C. Culp, T. Matsunaga, R. Porter, Effectiveness of lipid microbubbles and ultrasound in declotting thrombosis, Ultrasound Med. Biol. 31 (2005) 979–985.

[156] M. Ribo, C.A. Molina, B. Alvarez, M. Rubiera, J. Alvarez-Sabin, M. Matas, Intra-arterial administration of microbubbles and continuous 2-MHz ultrasound insonation to enhance intra-arterial thrombolysis, J. Neuroimaging 20 (2010) 224–227.

[157] R. Aaslid, T.M. Markwalder, H. Nornes, Noninvasive transcranial Doppler ultrasound recording of flow velocity in basal cerebral arteries, J. Neurosurg. 57 (1982) 769–774.

[158] M. Daffertshofer, A. Gass, P. Ringleb, M. Sitzer, U. Sliwka, T. Els, O. Sedlaczek, W. J. Koroshetz, M.G. Hennerici, Transcranial low-frequency ultrasound-mediated thrombolysis in brain ischemia: increased risk of hemorrhage with combined ultrasound and tissue plasminogen activator: results of a phase II clinical trial, Stroke 36 (2005) 1441–1446.

[159] M.A. Moehring, A. Voie, M.P. Spencer, D.W. Amory, A. Alexandrov, Investigation of transcranial Doppler (TCD) power output for potentiation of tissue plasminogen activator (tPA) therapy in stroke, Cerebrovascular Diseases 10 (2000).

[160] S. Behrens, K. Spengos, M. Daffertshofer, H. Schroeck, C.E. Dempfle, M. Hennerici, Transcranial ultrasound-improved thrombolysis: diagnostic vs. therapeutic ultrasound, Ultrasound Med. Biol. 27 (2001) 1683–1689.

[161] P. Cintas, F. Nguyen, A. Pavy le Traon, B. Boneu, V. Larrue, Enhancement of rtPA-induced thrombolysis by exposure to low-intensity, high-frequency ultrasound, Cerebrovascular Diseases 11 (2001) 20.

[162] P.P. Mohan, J.J. Manov, F. Contreras, M.E. Langston, M.H. Doshi, G. Narayanan, Ultrasound-Assisted Catheter-Directed Thrombolysis for Submassive Pulmonary Embolism, Vascular and Endovascular Surgery 52 (2018) 195–201.

[163] B. Scientific, EKOS™ Endovascular System, in, 2021.

[164] T. Richardson, D. Kerr, Skin-Related Complications of Insulin Therapy, Am. J. Clin. Dermatol. 4 (2003) 661–667.

[165] H.A.E. Benson, J.C. McElnay, R. Harland, Use of Ultrasound to Enhance Percutaneous Absorption of Benzydamine, Phys. Ther. 69 (1989) 113–118.

[166] K. Tachibana, Transdermal Delivery of Insulin to Alloxan-Diabetic Rabbits by Ultrasound Exposure, Pharm. Res. 9 (1992) 952–954.

[167] B. Kari, Control of Blood Glucose Levels in Alloxan-diabetic Rabbits by Iontophoresis of Insulin, Diabetes 35 (1986) 217.

[168] R. Brucks, M. Nanavaty, D. Jung, F. Siegel, The Effect of Ultrasound on the in Vitro Penetration of Ibuprofen Through Human Epidermis, Pharm. Res. 6 (1989) 697–701.

[169] S. Mitragotri, D. Blankschtein, R. Langer, Ultrasound-mediated transdermal protein delivery, Science 269 (1995) 850.

[170] E. Vranić, Sonophoresis-mechanisms and application, Bosnian Journal of Basic Medical Sciences 4 (2008) 25–32.

[171] K. Moriyama, N. Yui, Regulated insulin release from biodegradable dextran hydrogels containing poly(ethylene glycol), J. Control. Release 42 (1996) 237–248.

[172] S.H. Gehrke, L.H. Uhden, J.F. McBride, Enhanced loading and activity retention of bioactive proteins in hydrogel delivery systems, J. Control. Release 55 (1998) 21–33.

[173] F.P. Kennedy, Recent developments in insulin delivery techniques, Current status and future potential, Drugs 42 (1991) 213–227.

[174] I. Lavon, J. Kost, Mass transport enhancement by ultrasound in non-degradable polymeric controlled release systems, J. Control. Release 54 (1998) 1–7.

[175] Q. Wang, L. Wang, M.S. Detamore, C. Berkland, Biodegradable Colloidal Gels as Moldable Tissue Engineering Scaffolds, Adv. Mater. 20 (2008) 236–239.

[176] S.L. Tao, T.A. Desai, Microfabricated drug delivery systems: from particles to pores, Adv. Drug Deliv. Rev. 55 (2003) 315–328.

[177] R.M. Vlad, G.J. Czarnota, A. Giles, M.D. Sherar, J.W. Hunt, M.C. Kolios, High-frequency ultrasound for monitoring changes in liver tissue during preservation, Phys. Med. Biol. 50 (2005) 197–213.

[178] M.N. Kumar, R.A. Muzzarelli, C. Muzzarelli, H. Sashiwa, A.J. Domb, Chitosan chemistry and pharmaceutical perspectives, Chem. Rev. 104 (2004) 6017–6084.

[179] M.S. Shive, J.M. Anderson, Biodegradation and biocompatibility of PLA and PLGA microspheres, Adv. Drug Deliv. Rev. 28 (1997) 5–24.

[180] F. Danhier, E. Ansorena, J.M. Silva, R. Coco, A. Le Breton, V. Préat, PLGA-based nanoparticles: an overview of biomedical applications, J. Control. Release 161 (2012) 505–522.

[181] M. Mozafari, M. Shimoda, A.M. Urbanska, S. Laurent, Ultrasound-targeted microbubble destruction: toward a new strategy for diabetes treatment, Drug Discov Today 21 (2016) 540–543.

[182] I. Suarez Castellanos, A. Jeremic, J. Cohen, V. Zderic, Ultrasound Stimulation of Insulin Release from Pancreatic Beta Cells as a Potential Novel Treatment for Type 2 Diabetes, Ultrasound Med. Biol. 43 (2017) 1210–1222.

[183] WHO, Weekly epidemiological update on COVID-19 - 17 August 2021, in: Emergency Situational Updates, 2021.

[184] A. Cossarizza, S. De Biasi, G. Guaraldi, M. Girardis, C. Mussini, SARS-CoV-2, the Virus that Causes COVID-19: Cytometry and the New Challenge for Global Health, Cytometry A 97 (2020) 340–343.

[185] G.D. Zhu, J. Cao, Challenges and countermeasures on Chinese malaria elimination programme during the coronavirus disease, (COVID-19) outbreak, Zhongguo Xue Xi Chong Bing Fang Zhi Za Zhi 32 (2020) (2019) 7–9.

[186] A.E. Merkler, N.S. Parikh, S. Mir, A. Gupta, H. Kamel, E. Lin, J. Lantos, E. J. Schenck, P. Goyal, S.S. Bruce, J. Kahan, K.N. Lansdale, N.M. LeMoss, S. B. Murthy, P.E. Stieg, M.E. Fink, C. Iadecola, A.Z. Segal, M. Cusick, T. R. Campion Jr., I. Diaz, C. Zhang, B.B. Navi, Risk of Ischemic Stroke in Patients With Coronavirus Disease, (COVID-19) vs Patients With Influenza, JAMA Neurology 77 (2020) (2019) 1–7.

[187] S. Yaghi, K. Ishida, J. Torres, B. Mac Grory, E. Raz, K. Humbert, N. Henninger, T. Trivedi, K. Lillemoe, S. Alam, M. Sanger, S. Kim, E. Scher, S. Dehkharghani, M. Wachs, O. Tanweer, F. Volpicelli, B. Bosworth, A. Lord, J. Frontera, SARS-CoV-2 and Stroke in a New York Healthcare System, Stroke 51 (2020) 2002–2011.

[188] J.S. Ayres, A metabolic handbook for the COVID-19 pandemic, Nature, Metabolism 2 (2020) 572–585.

[189] D.R. Long, S. Gombar, C.A. Hogan, A.L. Greninger, V. Oreilly Shah, C. Bryson-Cahn, B. Stevens, A. Rustagi, K.R. Jerome, C.S. Kong, J. Zehnder, N.H. Shah, N. S. Weiss, B.A. Pinsky, J. Sunshine, Occurrence and Timing of Subsequent SARS-CoV-2 RT-PCR Positivity Among Initially Negative Patients, Clin. Infect. Dis. 72 (2020) 323–326.

[190] R. Weissleder, H. Lee, J. Ko, M.J. Pittet, COVID-19 diagnostics in context, Sci. Transl. Med. 12 (2020).

[191] FDA (2021).

[192] X. Xie, Z. Zhong, W. Zhao, C. Zheng, F. Wang, J. Liu, C.T. Chest, for Typical Coronavirus Disease, (COVID-19) Pneumonia: Relationship to Negative RT-PCR Testing, Radiology 296 (2020) (2019) E41–e45.

[193] P. Huang, T. Liu, L. Huang, H. Liu, M. Lei, W. Xu, X. Hu, J. Chen, B. Liu, Use of Chest CT in Combination with Negative RT-PCR Assay for the, Novel Coronavirus but High Clinical Suspicion, Radiology 295 (2020) (2019) 22–23.

[194] Y. Fang, H. Zhang, J. Xie, M. Lin, L. Ying, P. Pang, W. Ji, Sensitivity of Chest CT for COVID-19: Comparison to RT-PCR, Radiology 296 (2020) E115–e117.

[195] C.A. Raptis, M.M. Hammer, R.G. Short, A. Shah, S. Bhalla, A.J. Bierhals, P. D. Filev, M.D. Hope, J. Jeudy, S.J. Kligerman, T.S. Henry, Chest CT and Coronavirus Disease (COVID-19): A Critical Review of the Literature to Date, Am. J. Roentgenol. 215 (2020) 839–842.

[196] P.H. Mayo, R. Copetti, D. Feller-Kopman, G. Mathis, E. Maury, S. Mongodi, F. Mojoli, G. Volpicelli, M. Zanobetti, Thoracic ultrasonography: a narrative review, Intensive Care Med. 45 (2019) 1200–1211.

[197] F. Mojoli, B. Bouhemad, S. Mongodi, D. Lichtenstein, Lung Ultrasound for Critically Ill Patients, Am. J. Respir. Crit. Care Med. 199 (2019) 701–714.

[198] M. Demi, R. Prediletto, G. Soldati, L. Demi, Physical Mechanisms Providing Clinical Information From Ultrasound Lung Images: Hypotheses and Early Confirmations, IEEE Trans. Ultrason. Ferroelectr. Freq. Control 67 (2020) 612–623.

[199] G. Soldati, M. Demi, A. Smargiassi, R. Inchingolo, L. Demi, The role of ultrasound lung artifacts in the diagnosis of respiratory diseases, Expert Review of, Respir. Med. 13 (2019) 163–172.

[200] R. Inchingolo, A. Smargiassi, F. Mormile, R. Marra, S. De Carolis, A. Lanzone, S. Valente, G.M. Corbo, Look at the lung: can chest ultrasonography be useful in pregnancy? Multidisciplinary Respiratory Medicine 9 (2014) 32.

[201] Q.Y. Peng, X.T. Wang, L.N. Zhang, Findings of lung ultrasonography of novel corona virus pneumonia during the 2019–2020 epidemic, Intensive Care Med. 46 (2020) 849–850.

[202] E. Poggiali, A. Dacrema, D. Bastoni, V. Tinelli, E. Demichele, P. Mateo Ramos, T. Marcianò, M. Silva, A. Vercelli, A. Magnacavallo, Can Lung US Help Critical Care Clinicians in the Early Diagnosis of Novel Coronavirus (COVID-19) Pneumonia? Radiology 295 (2020) E6.

[203] G. Soldati, A. Smargiassi, R. Inchingolo, D. Buonsenso, T. Perrone, D.F. Briganti, S. Perlini, E. Torri, A. Mariani, E.E. Mossolani, F. Tursi, F. Mento, L. Demi, Is There a Role for Lung Ultrasound During the COVID-19 Pandemic? J. Ultrasound Med. 39 (2020) 1459–1462.

[204] K. Yasukawa, T. Minami, Point-of-Care Lung Ultrasound Findings in Patients with COVID-19 Pneumonia, The American Journal of Tropical Medicine and Hygiene 102 (2020) 1198–1202.

[205] G. Soldati, A. Smargiassi, R. Inchingolo, D. Buonsenso, T. Perrone, D.F. Briganti, S. Perlini, E. Torri, A. Mariani, E.E. Mossolani, F. Tursi, F. Mento, L. Demi, Proposal for International Standardization of the Use of Lung Ultrasound for Patients With COVID-19: A Simple, Quantitative, Reproducible Method, J. Ultrasound Med. 39 (2020) 1413–1419.

[206] R. Inchingolo, A. Smargiassi, F. Moro, D. Buonsenso, S. Salvi, P. Del Giacomo, G. Scoppettuolo, L. Demi, G. Soldati, A.C. Testa, The diagnosis of pneumonia in a pregnant woman with coronavirus disease, using maternal lung ultrasound, Am. J. Obstet. Gynecol. 223 (2020) (2019) 9–11.

[207] M. Attanasi, S. Pasini, A. Caronni, G.M. Pellegrino, P. Faverio, S. Di Pillo, M. M. Cimino, G. Cipolla, F. Chiarelli, S. Centanni, G.F. Sferrazza Papa, Inpatient Care during the COVID-19 Pandemic: A Survey of Italian Physicians, Respiration 99 (2020) 667–677.

[208] D. Pata, P. Valentini, C. De Rose, R. De Santis, R. Morello, D. Buonsenso, Chest Computed Tomography and Lung Ultrasound Findings in COVID-19 Pneumonia: A Pocket Review for Non-radiologists, Front Med (Lausanne) 7 (2020) 375.

[209] S.L. Archer, W.W. Sharp, E.K. Weir, Differentiating COVID-19 Pneumonia From Acute Respiratory Distress Syndrome and High Altitude Pulmonary Edema: Therapeutic Implications, Circulation 142 (2020) 101–104.

[210] H.M. DuBrock, M.J. Krowka, Bubble Trouble in COVID-19, Am. J. Respir. Crit. Care Med. 202 (2020) 926–928.

[211] S. Raevens, M.B. Fallon, Potential Clinical Targets in Hepatopulmonary Syndrome: Lessons From Experimental Models, Hepatology 68 (2018) 2016–2028.

[212] J. Santos, P. Young, I. Barjaktarevic, C. Lazar, I. Susanto, T. Wang, The successful use of inhaled nitric oxide in the management of severe hepatopulmonary syndrome after orthotopic liver transplantation, Case Reports Hepatol 2014 (2014), 415109.

[213] A.H. Katsanos, T. Psaltopoulou, T.N. Sergentanis, A. Frogoudaki, A.R. Vrettou, I. Ikonomidis, I. Paraskevaidis, J. Parissis, C. Bogiatzi, C. Zompola, J. Ellul, N. Triantafyllou, K. Voumvourakis, A.P. Kyritsis, S. Giannopoulos, A. W. Alexandrov, A.V. Alexandrov, G. Tsivgoulis, Transcranial Doppler versus transthoracic echocardiography for the detection of patent foramen ovale in patients with cryptogenic cerebral ischemia: A systematic review and diagnostic test accuracy meta-analysis, Ann. Neurol. 79 (2016) 625–635.

[214] L. O'Driscoll, Extracellular vesicles from mesenchymal stem cells as a Covid-19 treatment, Drug Discov Today 25 (2020) 1124–1125.

[215] K. Jayaramayya, I. Mahalaxmi, M.D. Subramaniam, N. Raj, A.A. Dayem, K. M. Lim, S.J. Kim, J.Y. An, Y. Lee, Y. Choi, A. Raj, S.G. Cho, B. Vellingiri, Immunomodulatory effect of mesenchymal stem cells and mesenchymal stem-cell-derived exosomes for COVID-19 treatment, BMB Reports 53 (2020) 400–412.

[216] V. Sengupta, S. Sengupta, A. Lazo, P. Woods, A. Nolan, N. Bremer, Exosomes Derived from Bone Marrow Mesenchymal Stem Cells as Treatment for Severe COVID-19, Stem Cells Dev. 29 (2020) 747–754.

[217] K. Kooiman, H.J. Vos, M. Versluis, N. de Jong, Acoustic behavior of microbubbles and implications for drug delivery, Adv. Drug Deliv. Rev. 72 (2014) 28–48.

[218] C. Baston, T.E. West, Lung ultrasound in acute respiratory distress syndrome and beyond, J Thorac Dis 8 (2016) E1763–E1766.

[219] A.P. Vincent Chan, Basics of Ultrasound Imaging, in: S.N. Narouze (Ed.), Atlas of Ultrasound-Guided Procedures in Interventional Pain Management, Springer-Verlag, New York, 2011, pp. 13–19.

[220] M.R. Carvalho, D. Lima, R.L. Reis, V.M. Correlo, J.M. Oliveira, Evaluating Biomaterial- and Microfluidic-Based 3D Tumor Models, Trends Biotechnol. 33 (2015) 667–678.

[221] H.-R. Moon, B. Han, 15 - Engineered tumor models for cancer biology and treatment, in: K. Park (Ed.), Biomaterials for Cancer Therapeutics (Second Edition), Woodhead Publishing, 2020, pp. 423–443.

[222] J.M. Long, D.M. Holtzman, Alzheimer Disease: An Update on Pathobiology and Treatment Strategies, Cell 179 (2019) 312–339.

[223] R.J. Bateman, C. Xiong, T.L.S. Benzinger, A.M. Fagan, A. Goate, N.C. Fox, D. S. Marcus, N.J. Cairns, X. Xie, T.M. Blazey, D.M. Holtzman, A. Santacruz, V. Buckles, A. Oliver, K. Moulder, P.S. Aisen, B. Ghetti, W.E. Klunk, E. McDade, R. N. Martins, C.L. Masters, R. Mayeux, J.M. Ringman, M.N. Rossor, P.R. Schofield, R.A. Sperling, S. Salloway, J.C. Morris, Clinical and Biomarker Changes in Dominantly Inherited Alzheimer's Disease, N. Engl. J. Med. 367 (2012) 795–804.

[224] B. Fonseca, C. Fonseca, M. Barros, M. White, V. Abhyankar, D. Borkholder, S. Balasubramaniam, Ultrasound-based Control of Micro-Bubbles for Exosome Delivery in Treating COVID-19 Lung Damage, in, arXiv, 2021.